Energy dependence of the fundamental parameters of the K^0-$\bar{K}^0$ system. I. Experimental analysis

S. H. Aronson
Physics Department, Brookhaven National Laboratory, Upton, New York 11973

G. J. Bock
Enrico Fermi Institute, University of Chicago, Chicago, Illinois 60637

Hai-Yang Cheng and Ephraim Fischbach
Physics Department, Purdue University, West Lafayette, Indiana 47907

(Received 2 December 1982)

An analysis of K^0 regeneration data from Fermilab in the energy range 30—110 GeV has been carried out to determine the K_L-K_S mass difference Δm, the K_S lifetime τ_S, and the *CP*-violation parameter η_{+-}. We find that the average values of Δm, τ_S, $\tan\phi_{+-}$, and $|\eta_{+-}|$ at Fermilab energies differ from the accepted low-energy ($\sim$5 GeV) values by approximately 4, 2, 3, and 9 standard deviations, respectively. As a consequence of the discrepancy between low-energy and high-energy values, an investigation of a possible energy dependence of the parameters was carried out. Using two different methods, the parameters were fitted to a form $x=x_0(1+b_x^{(N)}\gamma^N)$ where x is any of the parameters Δm, τ_S, $|\eta_{+-}|$, and $\tan\phi_{+-}$, $\gamma=E_K/m_K$ is the usual relativistic factor, and $N=1$ or 2. The resulting slope parameters $b_x^{(N)}$ differ from zero by 0—4 standard deviations depending on the parameter and on whether the low-energy value is included. The details of the fits are presented here, and a discussion is also given of new experiments which could check and extend the present results.

I. INTRODUCTION AND SUMMARY

In two recent papers[1-2] we have presented experimental limits on,[1] and explored the theoretical consequences of,[2] an energy dependence of the parameters of the K^0-$\bar{K}^0$ system. The object of the present paper and the following one[3] is to supply the details of the analyses in Refs. 1 and 2, and to suggest additional experiments to check and extend the results in Ref. 1. We begin by summarizing our notation and conventions.

We will be concerned in this paper with the following parameters of the K^0-$\bar{K}^0$ system: (a) The masses of K^0 and $\bar{K}^0$. In the absence of external forces acting on this system, and assuming CPT for the internal Hamiltonian (which we do), these masses should be the same and are denoted by m. (b) The masses of $K_L^0\equiv K_L$ and $K_S^0\equiv K_S$ which we denote by m_L and m_S, respectively. (c) The lifetimes of K_L and K_S, denoted by τ_L and τ_S, which are related to the corresponding widths Γ_L and Γ_S by $\tau_{L,S}=\hbar/\Gamma_{L,S}$. (d) The mass difference $\Delta m=m_L-m_S$. (e) The rate difference $\Gamma_L-\Gamma_S$. (f) The *CP*-violating parameters η_{+-} and η_{00} defined by

$$\eta_{+-}=|\eta_{+-}|e^{i\phi_{+-}}=\frac{A(K_L\to\pi^+\pi^-)}{A(K_S\to\pi^+\pi^-)}\ ,$$
$$\eta_{00}=|\eta_{00}|e^{i\phi_{00}}=\frac{A(K_L\to\pi^0\pi^0)}{A(K_S\to\pi^0\pi^0)}\ , \tag{1.1}$$

where the A's denote the amplitudes for the indicated decays. As we will discuss in Sec. II below, the energy dependence of $|\eta_{+-}|$ and ϕ_{+-} can be separately extracted from the data, and similarly for $|\eta_{00}|$ and ϕ_{00}. (g) The K_{l3} charge asymmetry δ defined by

$$\delta=\frac{\Gamma(K_L\to\pi^-l^+\nu)-\Gamma(K_L\to\pi^+l^-\bar{\nu})}{\Gamma(K_L\to\pi^-l^+\nu)+\Gamma(K_L\to\pi^+l^-\bar{\nu})}\ , \tag{1.2}$$

$$|K_L\rangle=(|p|^2+|q|^2)^{-1/2}[p|K^0\rangle+q|\bar{K}^0\rangle]\ ,$$
$$|K_S\rangle=(|p|^2+|q|^2)^{-1/2}[p|K^0\rangle-q|\bar{K}^0\rangle]\ , \tag{1.3}$$
$$\epsilon=1-q/p\ .$$

Although we cannot study the energy dependence of all of these parameters with the data currently available to us, future experiments will ultimately lead to a complete determination of the energy variation, if any, of all of the above quantities, and hence they are included here for the sake of completeness. (We will henceforth use "energy dependence" and "momentum dependence" interchangably, which is legitimate for the high-energy data discussed in Sec. II.)

The aim of the present analysis is to extract the slope parameters $b_x^{(N)}$ defined by

$$x=x_0(1+b_x^{(N)}\gamma^N)\ , \tag{1.4}$$

where x is any of the above parameters, and $\gamma=E_K/m=(1-\beta^2)^{-1/2}$ is the usual relativistic factor, which we have expressed in terms of the laboratory energy E_K of the kaons, or the kaon velocity β. N is an integer which for practical purposes will be restricted to 1 or 2 in the present analysis. It should be emphasized that Eq. (1.4) describes the behavior of the K^0-$\bar{K}^0$ parameters in a frame comoving with the kaon system, one in which these parameters should be constant. We will denote the slope parameters corresponding to $x=m$, m_L, m_S, Δm, Γ_L, Γ_S, $\Gamma_L-\Gamma_S$, τ_L, τ_S, $|\eta_{+-}|$, $\tan\phi_{+-}$, δ, and $\mathrm{Re}\epsilon$ by b_μ, $b_{\mu L}$, $b_{\mu S}$, b_Δ, $b_{\Gamma L}$, $b_{\Gamma S}$, b_Γ, $b_{\tau L}$, $b_{\tau S}$, b_η, b_ϕ, b_δ, and b_ϵ, respec-

TABLE I. Summary of data samples.

Target	p_K range (GeV/c)	t range[a] in τ_S units at 70 GeV/c	Number of $\pi^+\pi^-$ events at 0°	Number of $\pi\mu\nu$ events
1. Carbon (Ref. 5)	30—130	0—12	57 000	41 000
2. Hydrogen (Ref. 6)	30—130	0—11	50 000	35 000
3. Lead (Ref. 7)	30—100	0—1.3	460 000	

[a]The proper-time range depends on p_K because the data were collected over an evacuated region of fixed length behind the target. In fact, in both C and H two different length regions were used. The tabulated value is the longer one.

tively. Since these parameters are all expected to be small, it follows that x_0 is effectively the low-energy value of x, which we can identify with the result quoted by the Particle Data Group (PDG).[4] For the parameters of interest, the PDG values come from experiments at energies $E_K \lesssim 11$ GeV, whereas the present data derive from a series of regeneration experiments carried out at Fermilab[5-7] in the energy range $30 \leq E_K \leq 130$ GeV. Hence, the present analysis is the first attempt to extract the K^0-$\bar{K}^0$ parameters at high (Fermilab) energies.

In Sec. II, we present a detailed discussion of the analysis leading to the experimental results quoted in Ref. 1. We begin by reviewing the formalism describing K_S regeneration from a K_L beam, leading to Eqs. (2.11) and (2.11′) for the $\pi^+\pi^-$ decay rate dI^{+-}/dt. When the data of Refs. 5—7 (see also Table I) are fitted to Eqs. (2.11) or (2.11′), we obtain values of Δm, τ_S, $|\eta_{+-}|$, and ϕ_{+-} in the energy range 30—110 GeV. These results are given in Tables II and III, where they are also compared to the low-energy PDG values.

The observed difference between the present and the low-energy values of the K^0-$\bar{K}^0$ parameters prompted a search for an energy dependence of these parameters. Two methods of fitting the parameters Δm, τ_S, $|\eta_{+-}|$, and $\tan\phi_{+-}$ to expressions of the form given in Eq. (1.4) were used, and the results are given in Tables IV and V. In each method two sets of fits are presented for each slope parameter $b_x^{(N)}$, depending on whether the fit is constrained by the low-energy PDG value ("external fit") or not ("internal fit"). The internal fits are not subject to systematic errors associated with comparing data from different experiments; these show positive evidence of energy dependence (i.e., nonzero values of the $b_x^{(N)}$) at the level of up to 3σ in some cases. The external fits produce results which are always consistent with the internal fits and somewhat more statistically meaningful (up to 5σ to 7σ deviations from zero for some of the $b_x^{(N)}$).

Given the limited statistical significance of the present results, it is essential that further experiments be undertaken to verify and extend these results. A program to do this is discussed in Sec. III, which focuses not only on remeasurements of Δm, τ_S, and η_{+-}, but also on new experiments, such as measurements of the energy dependence of the charge asymmetry δ, and of τ_L.

In Appendix A, we review the kinematics of the regeneration process. Appendix B contains a detailed analysis of models of the strong-interaction regeneration phase ϕ_{21}. Over the interval $35 \leq E_K \leq 105$ GeV, the difference $(\phi_{21}-\phi_{+-})$ changes by (19.3 ± 6.4) degrees in hydrogen [see Eq. (B1)], whereas all of the models in Appendix B indicate that ϕ_{21} should change by $\lesssim 2°$. Taking at face value the results of Sec. II and these models, we are led to infer an energy dependence of ϕ_{+-} itself.

II. EXPERIMENTAL RESULTS

In order to study the parameters of the K^0-$\bar{K}^0$ system at very high energies, we have reanalyzed the data from a series of studies of K^0 coherent regeneration[8] at Fermilab. Two of us (S.H.A. and G.J.B.) have participated in all of these regeneration experiments, the results of which have been published previously.[5-7] In Sec. II A, the main features of K^0 regeneration are recapped and the available data are summarized. In Sec. II B, we discuss the details

TABLE II. Values of Δm, τ_S, $|\eta_{+-}|$, and $\tan\phi_{+-}$ obtained with fitting method B, using the published values of $|\rho|$, ϕ_ρ in carbon and hydrogen, with soft constraints equal to the published errors. Carbon results for $\tan\phi_{+-}$ are not quoted here, as explained in Appendix B.

Momentum (GeV/c)	Δm ($10^{10}\,\hbar\,\mathrm{sec}^{-1}$)		τ_S (10^{-10} sec)		$10^3\,\lvert\eta_{+-}\rvert$		$\tan\phi_{+-}$	χ^2 per degree of freedom	
	Hydrogen	Carbon	Hydrogen	Carbon	Hydrogen	Carbon	Hydrogen	Hydrogen	Carbon
30—40	0.530(38)	0.521(41)	1.017(155)	0.860(48)	2.30(21)	2.20(12)	1.003(378)	0.72	0.74
40—50	0.536(30)	0.516(24)	0.909(89)	0.895(18)	2.16(14)	2.08(12)	0.759(201)	0.91	1.19
50—60	0.508(23)	0.522(20)	0.899(43)	0.877(15)	2.08(7)	2.23(12)	0.976(198)	1.21	1.12
60—70	0.501(23)	0.518(20)	0.912(37)	0.884(13)	2.05(6)	2.15(8)	0.879(158)	1.20	0.62
70—80	0.508(40)	0.527(21)	0.942(49)	0.887(14)	2.15(9)	2.18(8)	0.821(170)	1.24	1.34
80—90	0.585(36)	0.511(31)	1.071(106)	0.908(17)	2.35(19)	2.09(11)	0.793(185)	1.48	1.11
90—100	0.498(57)	0.454(61)	0.968(79)	0.903(27)	2.07(16)	1.98(21)	0.372(145)	1.17	0.74
100—110	0.509(89)	0.470(100)	0.878(105)	0.879(59)	2.11(16)	2.16(50)	0.687(254)	1.09	1.16

TABLE III. Mean values of the parameters.

Parameter	Method A	Method B	Lead	PDG (Ref. 4)
$10^{-10}\Delta m$ ($\hbar$ sec^{-1})	0.482(14)	0.519(7)	0.442(61)	0.5349(22)
$10^{10}\tau_S$ (sec)	0.905(7)	0.892(6)	0.886(51)	0.8923(22)
$10^3\lvert\eta_{+-}\rvert$	2.09(2)	2.12(3)	2.17(21)	2.274(22)
$\tan\phi_{+-}$	0.709(102)	0.740(67)		0.986(41)

of the present analysis, including the use of "soft constraints" in the fit, the special case of extracting ϕ_{+-} from the data, and the differences between the two fitting methods used. In Sec. II C, we present the average (i.e., energy-independent) values for Δm, τ_S, $\lvert\eta_{+-}\rvert$, and ϕ_{+-} obtained from the present analysis and compare these with the accepted low-energy values. Section II D contains the results on the energy dependence of the parameters and discusses the statistical significance of these results. In Sec. II E, we discuss the relation of our results to previous work.

A. K^0 regeneration

The neutral-kaon states observed via their decays are the (approximate) CP eigenstates K_S, K_L composed of K^0 and $\bar{K}^0$ [see Eq. (1.3)],

$$K_{S,L}\simeq\frac{1}{\sqrt{2}}(K^0\mp\bar{K}^0)\ . \tag{2.1}$$

The K_S decays rapidly ($\tau_S\sim10^{-10}$ sec) and predominantly to two pions, while the K_L decays much more slowly ($\tau_L=581\tau_S$) and predominantly to 3π and $\pi l\nu$ states.

In their interaction with matter, neutral K's are most conveniently treated in terms of the strangeness eigenstates K^0 and $\bar{K}^0$. Let f ($\bar{f}$) be the elastic-scattering amplitude of K^0 ($\bar{K}^0$) on matter. It is easily seen from (2.1) that if $f\neq\bar{f}$, the CP state of a neutral-K beam is altered by its interaction with matter. Consider a pure K_L beam:

$$\lvert\Psi\rangle_{\rm in}\cong\frac{1}{\sqrt{2}}(\lvert K^0\rangle+\lvert\bar{K}^0\rangle)\ . \tag{2.2}$$

The state resulting from the interaction of $\lvert\Psi\rangle_{\rm in}$ in matter is

$$\lvert\Psi\rangle_{\rm out}\cong\frac{1}{\sqrt{2}}(f\lvert K^0\rangle+\bar{f}\lvert\bar{K}^0\rangle)\ . \tag{2.3}$$

Since from (2.1) we may write

$$\begin{aligned}\lvert K^0\rangle&\cong\frac{1}{\sqrt{2}}(\lvert K_S\rangle+\lvert K_L\rangle)\ ,\\ \lvert\bar{K}^0\rangle&\cong\frac{-1}{\sqrt{2}}(\lvert K_S\rangle-\lvert K_L\rangle)\ ,\end{aligned} \tag{2.4}$$

we get

$$\begin{aligned}\lvert\Psi\rangle_{\rm out}&\cong\frac{1}{\sqrt{2}}\left[\frac{f(\lvert K_S\rangle+\lvert K_L\rangle)}{\sqrt{2}}-\frac{\bar{f}(\lvert K_S\rangle-\lvert K_L\rangle)}{\sqrt{2}}\right]\\ &=\tfrac{1}{2}[(f+\bar{f})\lvert K_L\rangle+(f-\bar{f})\lvert K_S\rangle]\ .\end{aligned} \tag{2.5}$$

Thus, a K_S component proportional to $(f-\bar{f})$ is said to be regenerated in the interaction. In particular, if $f(\theta=0)\neq\bar{f}(\theta=0)$, then a regenerated K_S component coherent with the unscattered K_L beam is produced. Conventionally one relates the coherently regenerated K_S amplitude to the incident K_L amplitude by the regeneration parameter ρ,[8]

$$\lvert K_S\rangle=\rho\lvert K_L\rangle\ , \tag{2.6}$$

where, for a target of length L and having N nuclei per unit volume,

TABLE IV. Results of method A. (1) Internal fit. (2) External fit, with low-energy values at $E_K\cong5$ GeV: $\Delta m=(0.5349\pm0.0022)\times10^{10}\,\hbar$ sec^{-1}, $\tau_S=(0.8923\pm0.0022)\times10^{-10}$ sec, $\lvert\eta_{+-}\rvert=(2.274\pm0.022)\times10^{-3}$, $\tan\phi_{+-}=0.986\pm0.041$. (3) As in (2), except $\lvert\eta_{+-}\rvert=(1.95\pm0.03)\times10^{-3}$.

		Fits of the form $x=x_0(1+b_x^{(N)}\gamma^N)$						Energy-independent fit	
Parameter		x_0	$10^6b_x^{(2)}$	χ^2/dof	x_0	$10^4b_x^{(1)}$	χ^2/dof	x_0	χ^2/dof
$10^{-10}\Delta m$ ($\hbar$ sec^{-1})	(1)	0.557±0.036	−8.48± 2.89	521/484	0.620±0.066	−18.2 ±6.05	522/484	0.482±0.014	536/488
	(2)	0.535±0.002	−7.43± 1.48	533/488	0.535±0.002	−9.07±2.03	526/488	0.534±0.002	604/492
	(3)	0.534±0.002	−6.30± 1.46	550/488	0.535±0.002	−8.49±2.04	548/488	0.532±0.002	573/492
$10^{10}\tau_S$ (sec)	(1)	0.880±0.015	+ 1.77± 0.90	521/484	0.859±0.029	+ 4.35±2.58	522/484	0.905±0.007	536/488
	(2)	0.892±0.002	+ 1.27± 0.38	533/488	0.892±0.002	+ 1.47±0.56	526/488	0.895±0.002	604/492
	(3)	0.892±0.002	+ 0.99± 0.38	550/488	0.892±0.002	+ 1.27±0.57	548/488	0.893±0.002	573/492
$10^3\lvert\eta_{+-}\rvert$	(1)	2.14 ±0.04	−2.01± 0.86	521/484	2.21 ±0.07	−4.80±2.15	522/484	2.09 ±0.02	536/488
	(2)	2.23 ±0.02	−3.60± 0.52	533/488	2.26 ±0.02	−6.26±0.84	526/488	2.14 ±0.01	604/492
	(3)	2.07 ±0.02	−0.20± 0.62	550/488	2.03 ±0.03	+ 1.78±1.14	548/488	2.07 ±0.01	573/492
$\tan\phi_{+-}$	(1)	1.276±0.499	−33.7 ±12.3	521/484	2.071±1.840	−99.5 ±33.3	522/484	0.709±0.102	536/488
	(2)	0.954±0.048	−21.5 ± 7.0	533/488	0.966±0.052	−26.3 ±10.1	526/488	1.009±0.036	604/492
	(3)	1.033±0.052	−22.3 ± 6.7	550/488	1.009±0.054	−30.1 ±10.0	548/488	1.081±0.040	573/492

TABLE V. Results of method B. (1) Internal fit. (2) External fit, with low-energy values at $E_K \cong 5$ GeV: $\Delta m = (0.5349 \pm 0.0022) \times 10^{10}\ \hbar\,\text{sec}^{-1}$, $\tau_S = (0.8923 \pm 0.0022) \times 10^{-10}$ sec, $|\eta_{+-}| = (2.274 \pm 0.022) \times 10^{-3}$, $\tan\phi_{+-} = 0.986 \pm 0.041$. (3) As in (2), except $|\eta_{+-}| = (1.95 \pm 0.03) \times 10^{-3}$).

		Fits of the form $x = x_0(1 + b_x^{(N)}\gamma^N)$						Energy-independent fit	
Parameter		x_0	$10^6 b_x^{(2)}$	χ^2/dof	x_0	$10^4 b_x^{(1)}$	χ^2/dof	x_0	χ^2/dof
$10^{-10}\Delta m$	(1)	0.522±0.016	−0.33±1.66	6.4/14	0.525±0.030	−0.86±4.44	6.4/14	0.519±0.007	6.5/15
($\hbar\,\text{sec}^{-1}$)	(2)	0.535±0.002	−1.51±0.76	7.1/15	0.536±0.002	−2.49±1.19	6.6/15	0.534±0.002	10.8/16
$10^{10}\tau_S$	(1)	0.876±0.015	+0.94±0.83	7.7/14	0.862±0.028	+2.56±2.32	7.7/14	0.892±0.006	8.9/15
(sec)	(2)	0.892±0.002	+0.16±0.35	8.7/15	0.892±0.002	+0.14±0.56	8.9/15	0.892±0.002	8.9/16
$10^3\,\lvert\eta_{+-}\rvert$	(1)	2.140±0.061	−0.42±1.40	6.7/14	2.165±0.106	−1.45±3.63	6.6/14	2.124±0.027	6.8/15
	(2)	2.258±0.019	−2.73±0.69	10.7/15	2.277±0.021	−4.91±1.14	7.7/15	2.213±0.017	25.8/16
	(3)	1.986±0.027	+3.00±0.88	14.4/15	1.954±0.031	+6.12±1.56	10.4/15	2.047±0.020	25.6/16
$\tan\phi_{+-}$	(1)	1.052±0.154	−12.60±5.59	4.4/6	1.294±0.265	−28.8 ±13.3	4.8/6	0.740±0.067	9.5/7
	(2)	0.991±0.040	−11.26±2.93	4.6/7	1.013±0.043	−19.4 ±5.3	6.0/7	0.919±0.035	17.6/8

$$\rho = i\pi N \Lambda_S \alpha(L/\Lambda_S)\frac{f(0)-\bar{f}(0)}{k} . \tag{2.7}$$

$\Lambda_S = \beta\gamma\tau_S$ is the K_S mean decay length, k is the K^0 wave number, and

$$\alpha(L/\Lambda_S) = \frac{[1-\exp(-\frac{1}{2}+i\,\Delta m\,\tau_S)L/\Lambda_S]}{(\frac{1}{2}-i\,\Delta m\,\tau_S)} . \tag{2.8}$$

The function α describes the fact that within a target of finite length the regenerated K_S wave is decaying with characteristic length Λ_S and is also changing in phase relative to the K_L incident wave due to the K_L-K_S mass difference.

We now turn to the time evolution of the coherent K^0 state emerging from a material target at $t = 0$:

$$|\Psi(0)\rangle = |K_L\rangle + \rho\,|K_S\rangle . \tag{2.9}$$

We study the time evolution by looking at the time distribution of K^0 decays in the emergent beam. In particular, consider the decay to the $\pi^+\pi^-$ final state. K_S decays roughly $\frac{2}{3}$ of the time into this state; K_L also decays into $\pi^+\pi^-$ (violating CP invariance) with amplitude ratio η_{+-} relative to K_S:

$$\eta_{+-} = \frac{A(K_L \to \pi^+\pi^-)}{A(K_S \to \pi^+\pi^-)} . \tag{2.10}$$

Since the K_L,K_S components of the emergent beam are coherent, these decay amplitudes add, yielding for the $\pi^+\pi^-$ rate,[8]

$$dI^{+-}/dt = \Gamma_S^{+-} N_L \{\,|\rho|^2\exp(-t/\tau_S) + |\eta_{+-}|^2\exp(-t/\tau_L) + 2\,|\rho|\,|\eta_{+-}|\exp[(-t/2)(1/\tau_S + 1/\tau_L)]\cos(\Delta m\, t + \Phi)\} , \tag{2.11}$$

where N_L is the number of incident K_L's, and

$$\Gamma_S^{+-} = \Gamma(K_S \to \pi^+\pi^-) , \quad \Phi = \arg\rho - \arg\eta_{+-} \equiv \phi_\rho - \phi_{+-} .$$

Proper-time distributions of $K^0 \to \pi^+\pi^-$ events at $\theta = 0$ in ten momentum bins from 30 to 130 GeV/c have been fitted with Eq. (2.11) in Refs. 5 and 6 to obtain the momentum dependence of $|\rho|$ and ϕ_ρ in carbon and hydrogen, respectively. In the present analysis, we have used the same data and determined Δm, $|\eta_{+-}|$, and τ_S under conditions to be described in detail below. Additional assumptions about the regeneration parameter ρ enable us to isolate ϕ_{+-} as well.

In Ref. 7, a high-Z target (Pb) was used to study the electromagnetic interaction of K^0s. For this purpose the integrated rate of $K^0 \to \pi^+\pi^-$ decays over a relatively small time interval behind the target was studied. This sample provides much less information on the high-energy behavior of the K^0 parameters than the other experiments, which sampled decays over many decay lengths from the target. It is included where possible because a completely different apparatus and data-acquisition system were used; thus it constitutes an independent check on the results of the carbon and hydrogen data. Note that one can recast Eq. (2.11) in the form

$$dI^{+-}/dt = \Gamma_S^{+-} N_L\,|\eta_{+-}|^2[(|\rho|/|\eta_{+-}|)^2\exp(-t/\tau_S) + 1 + 2(|\rho|/|\eta_{+-}|)\exp(-t/2\tau_S)\cos(\Delta m\, t + \Phi)] , \tag{2.11'}$$

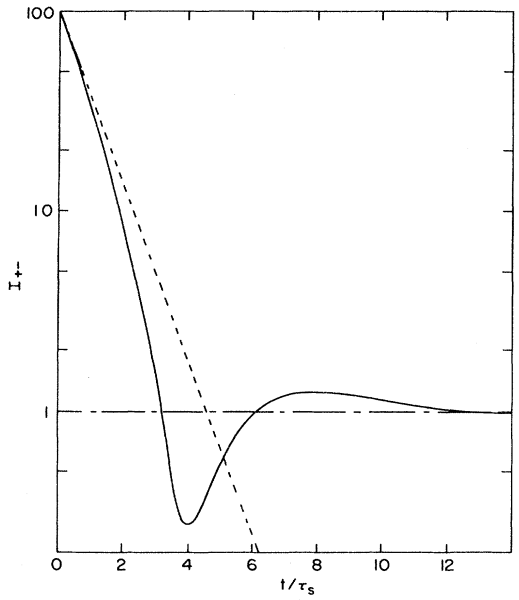

FIG. 1. A logarithmic plot of $I_{+-}(t)=(dI^{+-}/dt)/N_L|\eta_{+-}|^2$, where dI^{+-}/dt is defined in Eq. (2.11'). Here $|\rho|=10|\eta_{+-}|$, the dashed curve represents the first term in Eq. (2.11'), and the dot-dashed curve represents the second term. The solid curve represents the full expression and shows the effects of interference. The values of Δm, τ_S, and η_{+-} are taken from the Particle Data Group (Ref. 4).

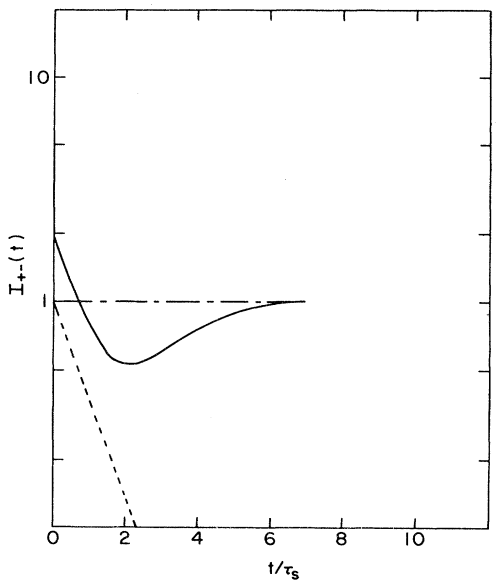

FIG. 2. A logarithmic plot of $I_{+-}(t)$ similar to Fig. 1, except with $|\rho|=|\eta_{+-}|$ (typical of the conditions in the hydrogen regeneration experiment—see Ref. 6).

where, in addition to factoring out $|\eta_{+-}|^2$, we eliminate τ_L for simplicity ($\tau_L \gg \tau_S$). The shape of the t distribution is given by the expression in square brackets in (2.11') (see Fig. 1). Even in the absence of knowledge of the flux we can determine the regeneration parameter ρ *relative to* the *CP*-violation parameter η_{+-}, i.e., the shape depends on $|\rho|/|\eta_{+-}|$ and on $\phi_\rho-\phi_{+-}$. In the present analysis, we wish to determine η_{+-} (among other parameters) without fixing ρ, so we need independent information on the factor outside the square brackets in (2.11'). The data samples used here contain $K^0\to\pi\mu\nu$ decays recorded simultaneously with the $K^0\to\pi^+\pi^-$ decays, and these are used to fix N_L. Table I summarizes the salient features of the three data samples.

B. Present analysis

The same computer program which fitted Eq. (2.11) to the proper-time distributions to produce the published regeneration parameters was used in the present analysis. The program searches for the minimum χ^2 point by varying the values of the parameters in the function which is being fitted to the data. While previously these fits were performed with Δm, τ_S, and η_{+-} fixed at their "known" values,[4] in the present case we allow the program to find a best value for these as well.

In practice, the data can support only a limited increase in the number of adjustable parameters. Correlations among parameters and statistical errors combine to limit the amount of information that can be extracted. In addition, we face the problem that the experiments were not designed to provide optimum information on the parameters of interest in the present analysis. We will return to this latter point in Sec. III, where a program of experiments is proposed to check and extend the present results.

The procedure followed to cope with the above-mentioned limitations is to allow Δm, τ_S, and $|\eta_{+-}|$ to be freely adjusted in finding the best fit, and to allow $|\rho|$ and ϕ_ρ to be adjusted subject to soft constraints which hold them near their published values. To be more precise, to softly constrain a parameter p to the value p_0 means to add to χ^2 a term of the form

$$(p-p_0)^2/\sigma^2 .$$

Thus, one unit is added to χ^2 when $|p-p_0|=\sigma$, where the softness of the constraint is governed by the magnitude of σ. We have performed the fits several times, with σ_ρ and σ_ϕ set to 1, 3, and 6 times the published errors on $|\rho|$ and ϕ_ρ. A fourth series of fits was performed with $|\rho|$ and ϕ_ρ fixed at their published values. These series of fits were performed in each of 10 momentum bins (10 GeV/c wide) from 30 to 130 GeV/c. A comparison of the best-fit values of $|\rho|$, ϕ_ρ, Δm, τ_S, and $|\eta_{+-}|$ in the different series of fits allowed us to check for (1) systematic or statistically significant deviations of $|\rho|$ and ϕ_ρ from their published values, and (2) correlations among the parameters which might show up as the constraints are made increasingly soft.

The results are that when the softest constraints on $|\rho|$ and ϕ_ρ are used (six times the published errors), and/or the highest momentum bins are studied ($p_K > 110$ GeV/c), some systematic deviations of the parameters or correlations among the parameters are observed. These problems reflect the fundamental limitations in the data mentioned earlier. At the highest momentum, the data spans the shortest proper-time interval and the regeneration amplitude is weakest: Figure 2 shows the shape of the $\pi^+\pi^-$

rate distribution for our hydrogen data at 125 GeV/c.

The highest momentum points do not significantly affect the results due to their limited statistical power, and they have been omitted from the quoted fits because of the observed correlations among the parameters. Thus, the analysis is performed in the momentum interval $30 \leq p_K \leq 110$ GeV/c. Similarly, the softest constraints yielded fits which show some drift in the parameters, especially Δm. No significant changes in the parameters are noted among the fits having the regeneration parameters fixed and those having σ_ρ, σ_ϕ equal to one or three times the published errors. We have chosen the fits with soft constraints equal to the published errors to quote here. In fact, the soft constraints contribute very little to χ^2 for the bulk of the data. The contribution from either the $|\rho|$ or ϕ_ρ term to the typical 10-GeV/c momentum bin below 110 GeV/c is ≤ 0.04, independent of the value of σ used. In other words, the data below 110 GeV/c could be used to determine *all* the parameters fairly well, although, as indicated above, some systematic drift is noted for the fits with the softest constraints. In one of the two fitting methods described below it was possible to perform fits with all constraints on $|\rho|$ removed. As we discuss in Sec. II D, qualitatively similar results for the K^0-$\bar{K}^0$ parameters emerge from these fits.

While we will be able to isolate values of Δm, τ_S, and the magnitude of η_{+-} in a straightforward way, subject only to the statistical limitations of our data, the phase ϕ_{+-} of η_{+-} requires special attention. A parameter which is of great interest in the unravelling of *CP* violation, ϕ_{+-} has been well measured at low energy.[4] The extraction of ϕ_{+-} from the present analysis is somewhat more difficult than for the other parameters, however, and the reason is apparent from inspection of Eq. (2.11): The interference term measures $\Phi \equiv \phi_\rho - \phi_{+-}$, the *phase difference* between the amplitudes ρ and η_{+-}. Hence ϕ_{+-} can be extracted only if ϕ_ρ is presumed to be known and vice versa. We note from Eqs. (2.7) and (2.8) that

$$\phi_\rho = \frac{\pi}{2} + \phi_{\text{geo}} + \phi_{21} , \tag{2.12a}$$

$$\phi_{21} = \arg[f(0) - \bar{f}(0)]/k , \tag{2.12b}$$

$$\phi_{\text{geo}} = \arg[\alpha(L/\Lambda_S)] , \tag{2.12c}$$

where α is defined in (2.8) and where the extra $\pi/2$ in (2.12a) comes from the overall factor of i in (2.7). Since the geometrical phase ϕ_{geo} is essentially determined by the known length of the target, it follows that a measurement of Φ gives one constraint relating the two unknown phases ϕ_{21} and ϕ_{+-}:

$$\Phi = \frac{\pi}{2} + \phi_{\text{geo}} + \phi_{21} - \phi_{+-} . \tag{2.13}$$

In the published regeneration results,[5-7] ϕ_{+-} was assumed to be independent of the incident kaon momentum, and hence was fixed at the low-energy value.[4] The experimental data for Φ were then used to extract ϕ_{21} as a function of momentum, and the results for ϕ_{21} were finally compared to theory. For purposes of the present analysis we will invert this procedure, and extract ϕ_{+-} from the data on Φ which are given in Table VI. To do so we must supply a theoretical model of ϕ_{21}, one which is independent of the phase information contained in the regeneration data. Several such models are discussed in detail in Appendix B. We will return to a discussion of the results of Appendix B in Secs. II C and II D.

TABLE VI. Experimental results for the quantity $(\pi/2 + \phi_{\text{geo}} - \Phi)$ in Eq. (2.13)

p_K (GeV/c)	$(\pi/2+\phi_{\text{geo}}-\Phi)$ (deg) Hydrogen	Carbon
35	172(10)	175(10)
45	164(6)	169(4)
55	171(4)	170(4)
65	168(3)	175(4)
75	166(4)	170(4)
85	165(5)	167(5)
95	147(6)	169(6)
105	161(9)	157(7)

As mentioned above, two different fitting methods were used to extract the K^0-$\bar{K}^0$ parameters of interest. We conclude Sec. II B with a comparison of the two methods (called A and B). First, we list the tests which are common to both methods which we applied to the data to look for systematic effects.

(1) The parameters have been fitted for individually as well as simultaneously. More precisely, we allowed each of the four parameters to seek its best value but allowed only one or two at a time to be energy-dependent. The results are that for τ_S and $|\eta_{+-}|$ the effects observed are unchanged from those of the simultaneous fits. For Δm and ϕ_{+-}, which appear together in Eq. (2.11) in the form

$$\cos(\Delta m\, t + \Phi) = \cos(\Delta m\, t + \phi_\rho - \phi_{+-}) ,$$

the results are that when Δm and ϕ_{+-} alone are allowed to be energy-dependent, the observed energy dependence is qualitatively similar to that observed when all four parameters are energy-dependent. The conclusion is that correlations among Δm, τ_S, $|\eta_{+-}|$, and ϕ_{+-}, though clearly present, are not the source of the results reported here.

(2) Fits have been repeated with reduced proper-time intervals to look for changes which might indicate systematic uncertainties in the spectrometer acceptance. No significant effects have been seen.

(3) A search was made for a momentum dependence of the reconstructed K^0 mass, which might indicate a systematic change of spectrometer acceptance or resolution with momentum. No drift in the value of m_S was found and no anomalous momentum dependence of the mass resolution was seen. Our results indicate that[9] (in GeV/c^2, with p_K in GeV/c)

$$m_S(p_K) - m_S(0) = (0.07 \pm 0.86) \times 10^{-4} p_K . \tag{2.14}$$

(4) As will be discussed in II D, an energy dependence in several K^0-$\bar{K}^0$ parameters is supported by the present data. A test was performed to suppress artificially the energy dependence of ϕ_{+-}. This was accomplished by deliberately distorting the spectrometer acceptance as a function of proper time from the regenerator to the spectrometer. The resultant suppression of the energy dependence of ϕ_{+-} was accompanied by almost no change in the energy dependence of the other parameters (indeed, the energy

dependence of Δm was slightly enhanced). This showed that residual errors in our understanding of the apparatus, if any, are not responsible for *all* the effects reported.

(5) In addition, extensive tests of these data were made prior to the publication of the regeneration results; these are discussed in Refs. 5–7.

The two fitting methods use the same input data, namely, the number of coherently regenerated $K^0 \to 2\pi$ events (plus normalizing $K^0 \to \pi\mu\nu$ events) in 10-GeV kaon energy bins and proper-time bins corresponding to 1 m intervals in the decay space.

Method A. In this case all energy and proper-time bins are fitted simultaneously to Eq. (2.11) with the ansatz that each of the parameters of interest has a form given by Eq. (1.4). Thus the output of such a fit is two numbers x_0 and $b_x^{(N)}$, representing the low-energy intercept and the slope, respectively, for each parameter x.

The chief advantage of method A is that the fitting is all done in a single step. Thus the correlations among the parameters which are apparent in the form of Eq. (2.11) can manifest themselves fully in the determination of the parameters. This method thus probably yields more unbiased estimates of the parameters than does method B as will be seen below. Another advantage of the one-step method A is that it makes it very easy to test the hypothesis of no energy dependence in any or all of the parameters, simply by constraining the relevant $b_x^{(N)}$'s to be zero. We discuss the results of testing these hypotheses in Sec. II D.

The disadvantage of method A is that one must assume the form of the energy dependence of each parameter [for example, Eq. (1.4)], rather than determining the value of each parameter in each energy bin and observing the energy dependence directly. As we will see, however, this is not a serious problem; the energy dependences are small and with the data available no differences can be found between the results with linear and quadratic forms.

Method B. The advantages and disadvantages of this method complement those of method A. Here we fit for the values x_i of all the parameters in each energy bin i. Then, in a separate fit, we determine x_0 and $b_x^{(N)}$ for each parameter x by fitting the values x_i with Eq. (1.4). Here each parameter is somewhat decoupled from the others, because in the second step [the fit to Eq. (1.4)] each parameter is fitted separately. The disadvantage is that this second step obscures the correlations in Eq. (2.11); the advantage is in being able to visualize how well the results conform to Eq. (1.4) for each parameter over energy.

We will present below results from both methods and comment on the comparison between them.

C. Results of the present analysis: Mean values of the parameters

In this section, we present the parameters Δm, τ_S, $|\eta_{+-}|$, and ϕ_{+-} extracted from the high-energy data as mean values (i.e., energy independent numbers). In method A, these are obtained by setting all the $b_x^{(N)}$'s equal to zero in the one-step fit. In method B, we obtain the value of each parameter in each 10-GeV energy bin and then find the weighted average over all energies.

Table II gives the bin-by-bin results of method B. The results are consistent between hydrogen and carbon regenerators. Table III presents the average values of the hydrogen and carbon results from method B above, together with the method A results, the results obtained from the lead data, and the accepted world averages.[4] The mean values are obtained in method A by performing the fits to the hydrogen and carbon data simultaneously with the constraints

$$b_\Delta^{(N)} = b_{\tau S}^{(N)} = b_\eta^{(N)} = b_\phi^{(N)} = 0 \ . \tag{2.15}$$

The lead results are obtained by analyzing the data as a single energy bin, $30 \le E_K \le 100$ GeV, because of the lesser statistical power of these data. One can conclude the following from Tables II and III.

(1) The agreement between different regenerator data samples is good. This is also the case for lead where, as noted above, a different spectrometer and data-analysis method were used.

(2) The agreement between method A and method B results is also good. This indicates that the correlations among the parameters, though present, are not the source of the effect reported here. Indeed, in method A, where the correlations are expected to be present in a more unbiased way, the effects (discussed immediately below and in Sec. II D) are somewhat more statistically significant.

(3) There is evidence of disagreement between the values of the parameters determined in the present analysis (with a mean kaon energy of about 70 GeV) and the accepted world averages,[4] for which the mean kaon energy is roughly 5 GeV. Taking the weighted mean of method A and lead values we find the discrepancies to be the following:

(i) Δm. The present analysis yields $(0.480 \pm 0.014) \times 10^{10}\ \hbar\ \text{sec}^{-1}$, which is 4 standard deviations below the world average.

(ii) τ_S. We obtain $(0.905 \pm 0.007) \times 10^{-10}$ sec, higher than the world average by 1.8 standard deviations.

(iii) $|\eta_{+-}|$. The result is $(2.09 \pm 0.02) \times 10^{-3}$; this is smaller than the world average by over 9 standard deviations.

A note on the subject of $|\eta_{+-}|$ is in order. The present world average is determined by a few recent experiments which disagree strongly with the previous body of results [$|\eta_{+-}|_{\text{old average}} = 1.95(3) \times 10^{-3}$ (Ref. 10)]. In addition, a more recent experiment at Brookhaven's Alternating Gradient Synchrotron[11] yields $|\eta_{+-}| = 1.97(10) \times 10^{-3}$, and one at Argonne's Zero Gradient Synchrotron[12] gives $|\eta_{+-}| = 2.25(5) \times 10^{-3}$. In light of the present confusion on this subject we will treat two cases of energy dependence in $|\eta_{+-}|$: We will use both the old and present world averages at low energy in conjunction with our own results in Sec. II D below.

(iv) $\tan\phi_{+-}$. The present result is 0.709 ± 0.102, or 2.7 standard deviations below the world average. Here we have used the method A result alone. The lead data, due to the small proper-time range, have very strong correlations between the phase Φ and other parameters, particularly Δm and $|\eta_{+-}|$, as can be seen in Table VII.[13] For this reason, and others discussed in II D and in Appendix B, we do not attempt to extract phase information from the lead data.

The discrepancies between Δm, $|\eta_{+-}|$, τ_S, and ϕ_{+-} and the established values are extremely tantalizing; how-

TABLE VII. The change in Φ in lead over the momentum interval $30 \leq p_K \leq 100$ GeV/c for different forms of Δm and $|\eta_{+-}|$ imposed on the fit.

Form of Δm, $\lvert\eta_{+-}\rvert$	$\Delta\Phi$(Pb)
1. $\Delta m = 0.540\times10^{10}\,\hbar\,\mathrm{sec}^{-1}$, $\lvert\eta_{+-}\rvert = 2.18\times10^{-3}$ (no energy dependence)	$(+2\pm3)^\circ$
2. $\Delta m = 0.534(1-1.5\times10^{-6}\gamma^2)\times10^{10}\,\hbar\,\mathrm{sec}^{-1}$ $\lvert\eta_{+-}\rvert = 2.26\times10^{-3}(1-2.7\times10^{-6}\gamma^2)$	$(+12\pm3)^\circ$
3. $\Delta m = 0.534(1-1.5\times10^{-6}\gamma^2)\times10^{10}\,\hbar\,\mathrm{sec}^{-1}$ $\lvert\eta_{+-}\rvert = 1.99\times10^{-3}(1+3.0\times10^{-6}\gamma^2)$	$(-7\pm3)^\circ$

ever, the following cautionary notes must be borne in mind.

(1) Drawing conclusions by comparing our results to those of other experiments at very different energies is subject to unknown systematic errors. For this reason the energy dependences of the parameters suggested by these discrepancies is investigated below *within our own data.*

(2) The value of $|\eta_{+-}|$ is not well understood even at low energy, as suggested above. The dangers of comparing our result to the low-energy average are especially acute for this parameter.

(3) The phase ϕ_{+-} cannot be extracted from the present data without theoretical input concerning the phases of strong amplitudes. Although our studies indicate (see Appendix B) that this is not a source of serious problems, we suggest in Sec. III that "cleaner" measurements of ϕ_{+-} at high energy are an important check on the present results.

(4) There are at present no high-energy data other than ours. (Data in the energy range 14—50 GeV from Serpukhov are discussed in II E.) Independent corroboration is needed, as emphasized in Sec. III.

D. Results of the present analysis: Energy dependence of the parameters

As discussed above, we are motivated to investigate the energy dependence of Δm, τ_S, $|\eta_{+-}|$, and ϕ_{+-} by the observed discrepancies from the accepted values of these parameters at low energy, but we try to avoid the problems of relating different data samples to one another. We do this in the present section by concentrating on the Fermilab data alone. We do, however quote the results of external fits (i.e., ones constrained by the PDG values) and comment on the comparison of external and internal fits.

The results of method A fits versus γ^2 and γ are presented in Table IV. The conditions under which these fits are produced are as follows.

(1) The values of $|\rho|$ for both hydrogen and carbon are softly constrained to the published[5,6] values with σ equal to the published errors in each energy bin.

(2) The values of ϕ_{21} are fixed according to the predictions of the DF model as discussed in Appendix B, from which we abstract the following salient points.

(a) In the usual Regge-pole description, the dominant contributions to the regeneration amplitude $[f(0)-\bar{f}(0)]/k$ in hydrogen arise from ω and ρ exchange. Since the Pomeron and f make no contributions, the regeneration amplitude is highly constrained in such models by virtue of the fact that the ω and ρ parameters can be determined by existing data on total cross sections. This is evidenced by the agreement among the predictions of the various models in Tables VIII (no abosrption) and IX (with absorption) for

TABLE VIII. Predictions of the simple Regge-pole model for the momentum dependence of the strong regeneration phase ϕ_{21}. $\Delta\phi_{21}=\phi_{21}(105\ \mathrm{GeV}/c)-\phi_{21}(35\ \mathrm{GeV}/c)$, and the numbers in parentheses give the errors in the least significant figures. Note that the entire momentum range $35 \leq p_K \leq 125$ GeV/c is used in fitting for the Regge parameters. Nonetheless, $\Delta\phi_{21}$ is calculated for the restricted range $35 \leq p_K \leq 105$ GeV/c since only this range will be used in Sec. II.

Model	$\alpha_\rho(0)$	$\alpha_\omega(0)$	β^ρ_{Kp} (mb)	β^ω_{Kp} (mb)	$\Delta\phi_{21}$ (deg)
Hendrick *et al.* (Ref. 26)	0.57(1)	0.43(1)	1.31(3)	7.97(13)	1.69
Bock *et al.* (Ref. 6) [fit (A)]	0.575(7)	0.44(1)	1.31(2)	7.34(30)	1.77
Bock *et al.* (Ref. 6) [fit (B)]	0.481(4)	0.41(1)	1.74(3)	8.17(34)	0.33
Diu *et al.* (Ref. 27)	0.51	0.443	2.50(7)	10.54(10)	0.35
This work	0.46	0.436(4)	5.51(29)	11.02(58)	0.17
	0.46	0.425(12)	2.67(29)	8.28(90)	0.12
	0.46	0.418(2)	1.61(2)	7.25(9)	0.09
	0.46	0.413(13)	1.24(11)	6.94(62)	0.08
	0.46	0.406(21)	1.08(15)	7.02(98)	0.09
	0.46	0.411(5)	0.81(3)	6.48(24)	0.05
	0.46	0.408(13)	0.64(5)	6.40(50)	0.05

TABLE IX. Predictions of the absorption model for the momentum dependence of the strong regeneration phase ϕ_{21}. $\Delta\phi_{21}=\phi_{21}(105\ \text{GeV}/c)-\phi_{21}(35\ \text{GeV}/c)$, and the numbers in parentheses give the errors in the least significant figures. The input parameters, in addition to $\alpha_\rho(0)$, are $\alpha'_\rho=0.8\ \text{GeV}^{-2}$, $\alpha'_\omega=1.1\ \text{GeV}^{-2}$, $\sigma_T(Kp)=48\ \text{GeV}^{-2}$, and $B\cong\frac{1}{2}(6+0.01p_K)\ \text{GeV}^{-2}$, where p_K is expressed in GeV/c.

$\alpha_\rho(0)$	$\alpha_\omega(0)$	$\tilde{\beta}^{\rho}_{Kp}$ (mb)	$\tilde{\beta}^{\omega}_{Kp}$ (mb)	$\Delta\phi_{21}$ (deg)
0.46	0.426(7)	6.90(54)	13.80(108)	1.55
0.46	0.405(3)	3.62(9)	11.22(28)	1.57
0.46	0.393(7)	2.25(11)	10.13(50)	1.51
0.46	0.389(53)	1.74(10)	9.74(56)	1.45
0.46	0.386(12)	1.45(10)	9.43(65)	1.43
0.46	0.381(10)	1.16(7)	9.28(56)	1.41
0.46	0.378(11)	0.90(6)	9.00(60)	1.38

$$\Delta\phi_{21}(\text{H})=\phi_{21}(\text{H};105\ \text{GeV}/c)-\phi_{21}(\text{H};35\ \text{GeV}/c)\ .$$

(b) All of these models indicate that $\Delta\phi_{21}(H)\lesssim 2^0$. By contrast, a linear fit to the experimental data of Ref. 6 gives $\Delta\phi_{21}^{\text{exp}}(H)=(19.3\pm6.4)^0$. Since these data were obtained under the assumption that ϕ_{+-} was constant (i.e., $\Delta\phi_{+-}=0$), it follows from Eq. (2.13) that over the interval $30\leq p_K\leq 110$ GeV/c in hydrogen, $\Phi(\text{H})-\phi_{\text{geo}}$ increases by $(19.3\pm6.4)^0$. If we now use any of the models of Appendix B to make a specific prediction for $\Delta\phi_{21}$ in Eq. (2.13), we find that the dominant contribution to $\Delta[\Phi(\text{H})-\phi_{\text{geo}}]$ comes not from $\Delta\phi_{21}(\text{H})$, but rather from $\Delta\phi_{+-}$. Thus, if the results of Appendix B are accepted, and are combined with the data for $\Phi(\text{H})$, a clear indication emerges that ϕ_{+-} is itself momentum-dependent.

(c) To quantify the momentum dependence of ϕ_{+-} we insert into Eq. (2.13) the experimental values for the expression $(\pi/2+\phi_{\text{geo}}-\Phi)$, which are given in Table VI, and the theoretical values of ϕ_{21} for the Diu–Ferraz de Camargo (DF) model[14,27] given in Table X. (As is evident from Tables VIII–X, all of the models we have considered lead to very similar results for ϕ_{+-}.)

(3) The K_L flux in each energy bin is constrained by the $K^0\to\pi\mu\nu$ data as discussed in II A.

(4) In fitting for the dependence of each parameter on γ and γ^2 we have used Eq. (1.4) with $N=1$ and 2, respectively.

Table V gives the analogous results for method B, where the conditions are the same as those enumerated above, except that the results for all the parameters are obtained in each energy bin (see Table II), and these are then fitted to Eq. (1.4) for each parameter in a separate step. Figures 3–6 show the method-B results for the fits versus γ^2. A number of points can be made in light of these results.

(1) The two methods agree well. The signs and magnitudes of the $b_x^{(N)}$'s are the same in A and B, both for internal and external fits. The differences are typically that method A gives somewhat larger and statistically more significant results for the $b_x^{(N)}$'s. We interpret these differences as being due to the different treatment of correlations in the two methods, as mentioned in Sec. II B; the correlations are clearly present and their effect is to enhance the results when they are included in the more complete way (i.e., in method A).

(2) For those internal fits where $b_x^{(N)}$ is significantly different from zero, the resulting intercepts x_0 are always in better agreement with the accepted low-energy values than were the mean values discussed in Sec. II C. This is most conveniently seen in Table IV, for method A, where the mean values are reproduced in the rightmost column. [For example, consider Δm: The energy-independent value is $0.482(14)\times10^{10}\ \hbar\,\text{sec}^{-1}$, or 3.8 standard devia-

TABLE X. Tabulation of ϕ_{21} as a function of p_K for the DF and absorption models. In the latter case the ratio of ω and ρ residues is 5.6. The remaining parameters in each model can then be obtained from Tables VIII and IX, respectively. The results are given for a hydrogen target.

	ϕ_{21} (deg)	
p_K (GeV/c)	DF model	Absorption model
35	−126.9	−126.9
45	−126.8	−126.5
55	−126.8	−126.3
65	−126.7	−126.0
75	−126.7	−125.8
85	−126.6	−125.7
95	−126.6	−125.6
105	−126.5	−125.4
115	−126.5	−125.3
125	−126.5	−125.2

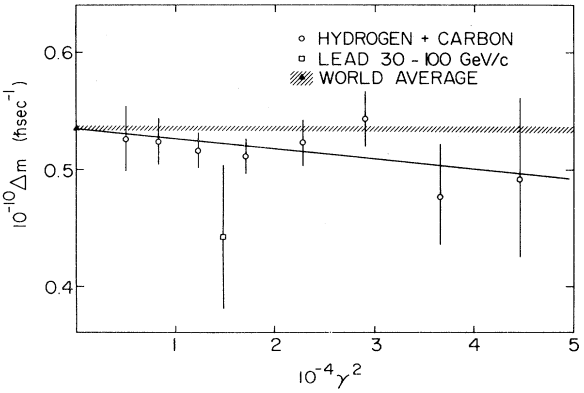

FIG. 3. A plot of the mass difference Δm versus γ^2. The data points are from Tables II and III and the solid line is the external fit versus γ^2 from Table V. The shaded band represents the world-average value of Δm (see Ref. 4).

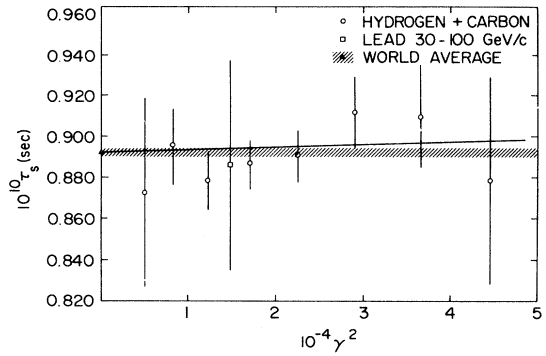

FIG. 4. A plot of the K_S lifetime τ_S versus γ^2. The data points are from Tables II and III and the solid line is the external fit versus γ^2 from Table V. The shaded band represents the world-average value of τ_S (see Ref. 4).

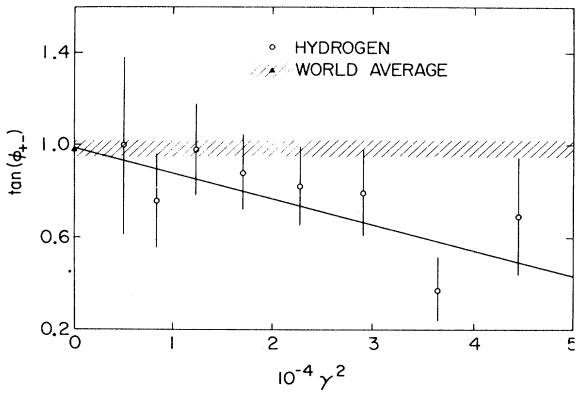

FIG. 6. A plot of $\tan\phi_{+-}$ versus γ^2. The data points are from Table II and the solid line is the external fit versus γ^2 given in Table V. The shaded band represents the world-average value of $\tan\phi_{+-}$ obtained from the value of ϕ_{+-} given in Ref. 4.

tions from the low-energy determination, whereas in the γ^2-dependent fit the intercept is seen to be $0.557(36)\times 10^{10}$ $\hbar\,\mathrm{sec}^{-1}$, or 0.6 standard deviations away from the low-energy value.] The only x_0 which remains more than 2 standard deviations from the accepted value in the energy-dependent fits is in the case of $|\eta_{+-}|$, where the confusion over the low-energy value itself has already been noted.

Another way of saying this is that the energy dependence seen within the Fermilab data is consistent with that implied by the comparison of the high- and low-energy determinations of the parameters. This can also be seen by comparing the internal fits with the external ones. Setting the case of $|\eta_{+-}|$ aside for the moment, we see good agreement in all cases between the internal and external determinations of the $b_x^{(N)}$'s. Typically, the external value is consistent with, and somewhat more statistically significant than, the internal value.

(3) Returning to $|\eta_{+-}|$, we have two external fits to compare to the internal one. This comparison, plus an inspection of the quality of the two external fits favors very slightly the present world-average value of $|\eta_{+-}|$, but the fits are acceptable in all cases. A stronger but still inconclusive indication is the agreement in the sign of $b_\eta^{(N)}$ between the internal fit and the external fit constrained by the present world average.

We can assess the significance of these results further by using the data to test the hypothesis of no energy dependence in any of the parameters. This can be done very straightforwardly in method A simply by performing the fit subject to the four constraints

$$b_\Delta = b_{\dot{r}S} = b_\eta = b_\phi = 0 \,. \tag{2.16}$$

This is the energy-independent fit presented in the rightmost column of Table IV, while the fits without the four constraints (2.16) are the ones we have been discussing and appear in the other columns in that table.

The difference in the χ^2 for these fits is the statistic used:

$$\Delta\chi^2 = \chi^2(\text{all } b's = 0) - \chi^2(b's \text{ free}) \,. \tag{2.17}$$

We expect[15] that since the four constraints (2.16) comprise the hypothesis under test, that $\Delta\chi^2$ should itself have a χ^2 distribution for 4 degrees of freedom. Taking as an example the internal γ^2 fit and comparing to the energy-independent fit we find $\Delta\chi^2 = 15$. Thus the hypothesis of no energy dependence is rejected by the Fermilab data alone with C.L. $\gg 99\%$. Similar results are obtained with the γ-dependent fit and even stronger statements can be made on the basis of $\Delta\chi^2$ from the external fits. We note once again, however, that because of the systematic uncertainties in combining the low- and high-energy results we stress the internal fit values.

We conclude this section with a discussion of three additional checks on the methods used in the present analysis.

(*i*) *Soft constraints.* As mentioned in Sec. II B, the effects of applying soft constraints to the regeneration parameters have been checked by removing these constraints in the following way. We fitted the data using method A with the soft constraints on $|\rho|$ completely removed. Re-

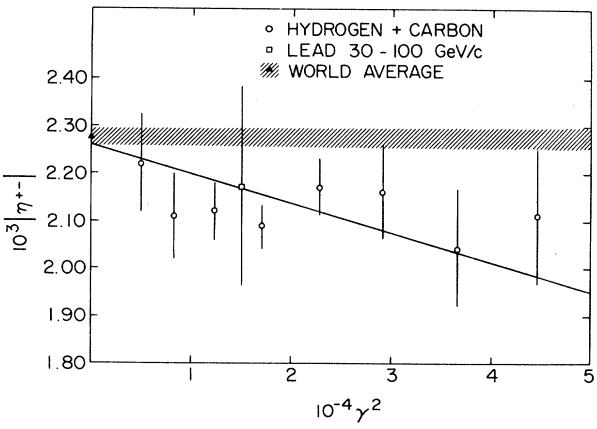

FIG. 5. A plot of the magnitude of the *CP*-violation parameter η_{+-}. The data points are from Tables II and III and the solid line is the external fit versus γ^2 from Table V. The shaded band represents the present world-average value of $|\eta_{+-}|$ (see Ref. 4).

TABLE XI. Results of additional internal fits using method A. These fits are discussed at the end of Sec. II D. Unless specified, all conditions are as in the fits in Table IV. (1) Fits with soft constraints on $|\rho|$ removed. (2) Fits in the range $30 \leq E_K \leq 130$ GeV.

Parameter		Fits of the form $x=x_0(1+b_x^{(2)}\gamma^2)$ x_0	$10^6 b_x^{(2)}$	χ^2/dof	Energy-independent fit x_0	χ^2/dof
$10^{-10}\,\Delta m$	(1)	0.552±0.045	−6.58± 3.44	515/484	0.494±0.018	531/488
($\hbar$ sec^{-1})	(2)	0.547±0.033	−7.63± 2.68	628/593	0.480±0.014	644/597
$10^{10}\,\tau_S$	(1)	0.881±0.022	+ 1.09± 1.13	515/484	0.898±0.009	531/488
(sec)	(2)	0.880±0.014	+ 1.74± 0.79	628/593	0.905±0.006	644/597
$10^3\,\lvert\eta_{+-}\rvert$	(1)	2.16 ±0.05	−2.96± 1.06	515/484	2.08 ±0.02	531/488
	(2)	2.14 ±0.03	−1.96± 0.75	628/593	2.09 ±0.02	644/597
$\tan\phi_{+-}$	(1)	1.159±0.619	−18.6 ±22.6	515/484	0.835±0.166	531/488
	(2)	1.166±0.406	−32.4 ±12.4	628/593	0.694±0.098	644/597

call that in the case of the phase ϕ_ρ, the relevant measured quantity is $\Phi=\phi_\rho-\phi_{+-}$, and that in method A ϕ_ρ was set to the DF-model prediction with ϕ_{+-} free to assume its best value. Thus, in effect, $|\rho|$ and Φ are fitted without soft constraints in the present case.

The results for the γ^2-dependent internal fit are shown in the entries marked (1) in Table XI. These are to be compared with the entries marked (1) in Table IV. The agreement is good, confirming the statement made in Sec. II B that the data determine all the parameters reasonably well.

(ii) $E_K > 110$ GeV. The highest-energy bins have been excluded from all fits for the reasons stated in Sec. II B. As a check on the effect of including these bins, fits were performed over the entire interval $30 \leq p_K \leq 130$ GeV/c. These results are also presented in Table XI, under the entries labeled (2). These are also in good agreement with the Table IV values. Method A might well be expected to account properly for the large correlations among parameters at the highest energy (noted in Sec. II B). However, it is fair to point out that the limited statistical weight of these bins (due to the rapidly falling K_L energy spectrum) is equally likely to account for their small effect on the results. In any case, it is clear that exclusion of these bins in most of the fits has not made a noticeable difference in our conclusions.

(iii) $K^0\to\pi\mu\nu$ normalization. As was mentioned in connection with Eq. (2.11′), the flux determination with $K^0\to\pi\mu\nu$ events greatly enhances the analysis of $K^0\to\pi^+\pi^-$. To study the possibility of a systematic discrepancy between the $\pi\mu\nu$ and $\pi^+\pi^-$ data samples, additional fits were carried out in which the flux calculation was changed by ± 10% relative to that used in all other fits.

The results are presented in Table XII and are discussed much more fully in Sec. II E, in a somewhat different context. For the present purposes we can conclude that the parameters are well behaved as the normalization is artificially changed. In particular, the energy dependences (i.e., the values of the b_x's) are qualitatively unchanged, and are thus unlikely to arise as an artifact of such systematic errors.

E. Relation of the present results to previous work

Given the indication of energy dependence in the Fermilab data, we can ask whether other indications of such an effect should be present in the published record.

TABLE XII. Dependence of the $K^0-\bar{K}^0$ parameters on $\Gamma_L^{\mu 3}$. For each parameter $x=x_0\,(1+b_x^{(2)}\gamma^2)$, the entries in lines (a)–(c) of the table give x_0 and $b_x^{(2)}$ corresponding to $\Gamma_L^{\mu 3}$, 0.9 $\Gamma_L^{\mu 3}$, and 1.1 $\Gamma_L^{\mu 3}$. Lines (d)–(f) give the analogous results for the case when all the slope parameters are set equal to zero.

	Δm_0 ($10^{10}\,\hbar$ sec^{-1})	$-b_\Delta$	τ_{S0} (10^{-10} sec)	$b_{\tau S}$	$10^3\,\lvert\eta_{+-}\rvert_0$	$-b_\eta$	$\tan(\phi_{+-})_0$	$-b_\phi$
(a) $\Gamma_L^{\mu 3}$	0.557(36)	8.48(289)	0.880(15)	1.77(90)	2.14(4)	2.01(86)	1.276(499)	33.7(123)
(b) 0.9 $\Gamma_L^{\mu 3}$	0.603(32)	8.14(238)	0.852(13)	2.03(79)	2.00(3)	2.24(80)	2.491(1109)	28.0(98)
(c) 1.1 $\Gamma_L^{\mu 3}$	0.504(42)	7.93(368)	0.913(20)	1.34(111)	2.29(4)	1.80(97)	0.654(345)	46.6(232)
(d) $\Gamma_L^{\mu 3}$	0.482(14)		0.905(7)		2.09(2)		0.709(102)	
(e) 0.9 $\Gamma_L^{\mu 3}$	0.524(13)		0.880(6)		1.94(1)		1.210(140)	
(f) 1.1 $\Gamma_L^{\mu 3}$	0.441(16)		0.933(8)		2.24(2)		0.362(97)	

In the published results on regeneration in hydrogen, based on these data,[6] it was noted that good fits were obtained only with values of $|\eta_{+-}|$ lower than the world average, and results were presented from two sets of fits with $|\eta_{+-}| = 2.15\times10^{-3}$ and 2.27×10^{-3}. Independently, hydrogen regeneration results from Serpukhov[16] at a mean K^0 momentum of about 32 GeV/c were also reported to require $|\eta_{+-}| = 2.15(14)\times10^{-3}$ for good fits. In the carbon data, acceptable fits were obtained and published using $|\eta_{+-}| = 2.27\times10^{-3}$. However, the value $|\eta_{+-}|$ is largely determined by the $K^0\to\pi\mu\nu$ normalizing events and, as can be seen from Table II, the carbon data "prefers" a lower value of $|\eta_{+-}|$.[17] Similar comments apply to the lead sample.

In addition, during the carbon regeneration experiment at Fermilab,[5] some data were taken with no regenerator in the K_L beam. The ratio of $K_L\to\pi^+\pi^-$ and $K_L\to\pi\mu\nu$ rates measures $|\eta_{+-}|^2$. The quoted result for $|\eta_{+-}|$ from this sample is[18]

$$|\eta_{+-}| = (2.200\pm0.030)\times10^{-3}\,, \tag{2.18}$$

which is about 2.5 standard deviations below the accepted low-energy value. It should be noted that this determination does not rely on knowing the regeneration amplitude, and that these CP-violating $\pi^+\pi^-$ decays have a proper-time distribution quite different from Eq. (2.11). Thus this result, although from the same experiments quoted throughout, is really a quite independent determination of $|\eta_{+-}|$. If we assume that the result in (2.18) corresponds to an average momentum of 70 GeV/c, then we can infer b_η by comparing (2.18) to the low-energy PDG value.[4] We find

$$b_\eta^{(2)} = -(1.64\pm0.81)\times10^{-6}\,, \tag{2.19}$$

in reasonably good agreement with the results of Table V.

It must be emphasized at this point that if the fundamental parameters of the K^0–$\bar{K}^0$ system are indeed energy-dependent, then care must be exercised in comparing different determinations of the same quantities. Consider, for example, the method of Ref. 18 in which $|\eta_{+-}|^2$ is determined via

$$|\eta_{+-}|^2 = \frac{\Gamma_L^{+-}}{\Gamma_S^{+-}} = \left[\frac{\Gamma_L^{+-}}{\Gamma_L^{\mu3}}\right]\left[\frac{\Gamma_L^{\mu3}}{\Gamma_S^{+-}}\right], \tag{2.20}$$

where $\Gamma_{L,S}^j$ denote the partial widths for the decay of $K_{L,S}$ into the mode j ($\pi^+\pi^-$ or $\pi\mu\nu$). In practice, the first ratio is measured directly, while the second is taken from the PDG.[4] Since Γ_S is energy-dependent, it is natural to suppose that the partial widths $\Gamma_{L,S}^j$ are as well. It follows that since the ratio $\Gamma_L^{\mu3}/\Gamma_S^{+-}$ is not actually measured at Fermilab energies, the result quoted in Eq. (2.18) may not represent the full energy dependence of $|\eta_{+-}|^2$. The most conservative interpretation of Eqs. (2.18) and (2.19) is that they describe the energy dependence of the ratio $\Gamma_L^{+-}/\Gamma_L^{\mu3}$, which is the quantity directly measured, and not that of $|\eta_{+-}|^2$. As we will see shortly, the same problem affects the present results as well. Since different partial widths $\Gamma_{L,S}^j$ may be expected to have different energy dependences, as we discuss in more detail in Ref. 3, it also follows that a different numerical result for $|\eta_{+-}|^2$ could be obtained if the 3π mode were used instead of the $\mu3$ mode, for example.

We now demonstrate that the same problem also affects the present determination of $|\eta_{+-}|$. Returning to Eq. (2.11), we see that in order to extract $|\eta_{+-}|^2$, it is necessary to know N_L, the number of incident K_L, which is measured by monitoring the number of $K_{\mu3}$ events:

$$\frac{dI^{\mu3}}{dt} = \Gamma_L^{\mu3} N_L e^{-\Gamma_L t} \simeq \Gamma_L^{\mu3} N_L \tag{2.21}$$

and hence,

$$N_L = \frac{1}{\Gamma_L^{\mu3}}\frac{dI^{\mu3}}{dt}\,. \tag{2.22}$$

If we focus on the term proportional to $|\eta_{+-}|^2$ in Eq. (2.11) we have

$$\begin{aligned}\frac{dI^{+-}}{dt} &= N_L\Gamma_S^{+-}|\eta_{+-}|^2+\cdots \\ &= \frac{\Gamma_S^{+-}}{\Gamma_L^{\mu3}}\frac{dI^{\mu3}}{dt}|\eta_{+-}|^2+\cdots\,,\end{aligned} \tag{2.23}$$

and hence,

$$|\eta_{+-}|^2 = \left[\frac{dI^{+-}/dt}{dI^{\mu3}/dt}\right]\left[\frac{\Gamma_L^{\mu3}}{\Gamma_S^{+-}}\right] = \left[\frac{\Gamma_L^{+-}}{\Gamma_L^{\mu3}}\right]\left[\frac{\Gamma_L^{\mu3}}{\Gamma_S^{+-}}\right]. \tag{2.24}$$

Comparing Eqs. (2.20) and (2.24), we see that the present method is equivalent in principle to that of Ref. 18, and hence suffers from the same problems discussed earlier. In practice, of course, one cannot simply isolate $|\eta_{+-}|^2$ as in Eq. (2.23) due to correlations among the various terms in Eq. (2.11). For this reason, if $\Gamma_L^{\mu3}$ were in fact energy dependent, the effect on $|\eta_{+-}|^2$ of neglecting this dependence would be different in these two methods. Specifically, let us suppose that $\Gamma_L^{\mu3}$ changed by a fractional amount $2\delta_{\mu3}$ over the energy range $35 \le E_K \le 105$ GeV:

$$\Gamma_L^{\mu3}\to\Gamma_L^{\mu3}(1+2\delta_{\mu3})\,. \tag{2.25}$$

Then, from Eq. (2.20), we see that the change in $|\eta_{+-}|$ would be

$$|\eta_{+-}|\to|\eta_{+-}|(1+\delta_{\mu3})\,. \tag{2.26}$$

To study the sensitivity of the present method to a possible energy variation of the normalizing $K_{\mu3}$ events, we changed $\Gamma_L^{\mu3}$ in method A by $\pm10\%$ from its nominal PDG value,[4] and the results are given in Table XII. On the basis of Eq. (2.26), we would have expected $|\eta_{+-}|$ to change by $\pm5\%$, but we see from Table XII that the variation was somewhat larger, typically $\pm7\%$. This may explain why the results for b_η in Table V are larger in magnitude than the value (2.19) inferred from Ref. 18. At the same time these results may also be hinting at a possible energy variation of $\Gamma_L^{\mu3}$. We note, incidentally, that the slope parameters are not especially sensitive to a change in $\Gamma_L^{\mu3}$, which suggests that the observed nonzero values of the $b_x^{(N)}$ are not a consequence of some error in determining N_L.

We now consider the phase ϕ_{+-} in the context of published work. Figure 7 contains a compendium of results on ϕ_{21} versus p_K in hydrogen and deuterium.[19] These data are mostly from coherent regeneration experiments[20] and

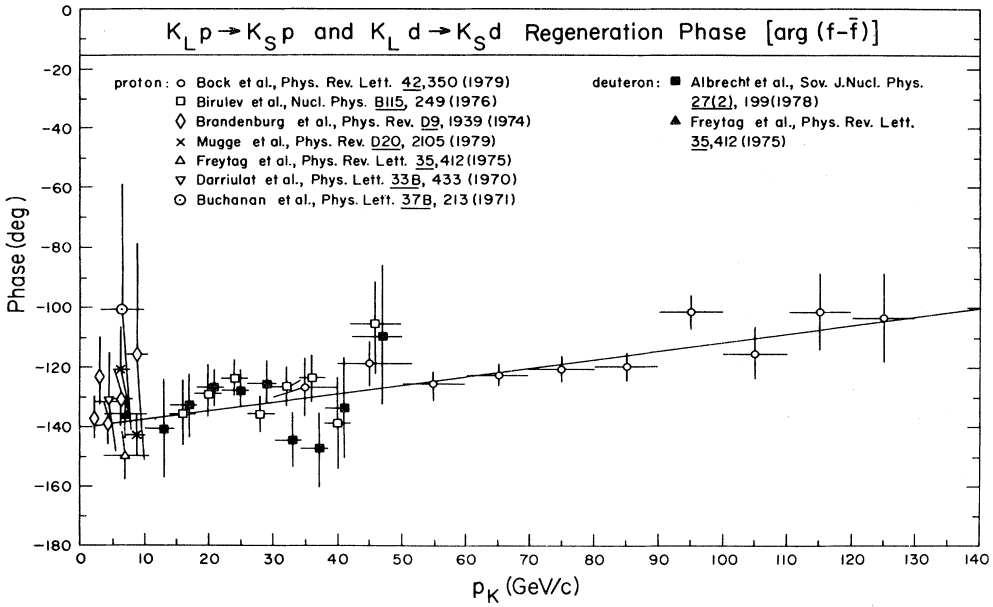

FIG. 7. A plot versus kaon momentum of $\phi_{21}=\arg[f(0)-\bar{f}(0)]$ for hydrogen and deuterium targets, adapted from Kelly *et al.* (Ref. 4). The straight line is a fit using only the data of Bock *et al.* (Ref. 6).

yield results for ϕ_{21} on the assumption that $\phi_{+-}=$constant$=45°$. Indeed, if these data points from hydrogen regeneration experiments are fitted to a form linear in p_K, the result is

$$\phi_{21}=(-140.6\pm4.3)°+(0.29\pm0.06)°p_K,$$
$$\chi^2=12.2\ (19\text{ degrees of freedom}), \tag{2.27}$$

where p_K is in GeV/c. Thus a good fit is obtained and leads to a change of ϕ_{21} of roughly 25° over the momentum range of the Fermilab data. By contrast, imposing the constraint that $\phi_{21}=$constant leads to

$$\phi_{21}=(-122.1\pm1.5)°,$$
$$\chi^2=33.0(20\text{ degrees of freedom}), \tag{2.28}$$

which is not a good fit (C.L. $<5\%$).

We conclude the discussion of ϕ_{+-} by focusing on a comparison of the high-energy results of Ref. 6 to those of Birulev *et al.*,[16] which is the only other experiment at energies high enough to be useful. Since the errors on ϕ_{21} from this experiment are relatively large compared to those of Ref. 6, we will simply use the average value of ϕ_{21}, $\langle\phi_{21}\rangle$, at an average momentum of 32 GeV/c. $\langle\phi_{21}\rangle$ can be extracted from Eq. (19) of their paper, which exhibits the corrections that must be applied to their published value to incorporate the revised values of τ_S, Δm, and ϕ_{+-}. We find

$$\langle\phi_{21}\rangle_{\text{Birulev}}=-(128.7\pm5)°. \tag{2.29}$$

Using Eq. (B1), the value of $\langle\phi_{21}\rangle$ we would expect at 32 GeV/c is

$$\langle\phi_{21}\rangle=-(130.7\pm7.2)°, \tag{2.30}$$

in excellent agreement with the Birulev result. A related indication of support in the Birulev data for the variation of ϕ_{21} in Eq. (B1) comes from a comparison of Eq. (2.29) with the analogous average of the data of Ref. 6 in the range $35\le p_K\le125$ GeV/c:

$$\langle\phi_{21}\rangle_{\text{Bock}}=-(120.3\pm1.7)°. \tag{2.31}$$

Assuming that the Bock result corresponds to an average momentum of 70 GeV/c, we see from Eqs. (2.29) and (2.31) that $\langle\phi_{21}\rangle$ has increased by $\sim8.4°$ over the interval of 30—70 GeV/c. This is substantially larger than can be accounted for by existing Regge-pole models unless ϕ_{+-} itself is also momentum-dependent.

III. SUGGESTED PROGRAM OF EXPERIMENTS TO CHECK THE PRESENT ANALYSIS

The experimental results quoted in this paper are of limited statistical significance. The evidence of a positive effect in the energy dependences of Δm, τ_S, $|\eta_{+-}|$, and ϕ_{+-} is extremely tantalizing but not conclusive. The evidence consists of $b_x^{(N)}$'s which are different from zero by at most 3 standard deviations (see Tables IV and V). Greater statistical significance is obtained only by the inclusion in the fits of the low-energy values, which opens the analysis to the risk of unknown systematic errors. The energy dependence of ϕ_{+-}, the most consistent positive result in all our fits, is subject to some uncertainty due to strong-interaction effects, as we discuss in Sec. II. It is thus evident that our results require corroboration from other workers.

The most obvious approach is to measure Δm, τ_S, $|\eta_{+-}|$, and ϕ_{+-} in high- (and low-) energy experiments properly designed to optimize the distribution of data for high precision in these parameters. In particular, experiments in which the regeneration phenomenon is absent (or

cancels out of the analysis) would not be subject to the uncertain contributions of strong interactions, as is the ϕ_{+-} determination in the present analysis. We consider very briefly below experiments to remeasure the K^0 parameters, concentrating on the high-energy versions.

(1) Δm. The mass difference has been measured precisely at low energy ($\langle E_K \rangle \sim 5$ GeV) with the so-called gap method[21] or a variant[22] thereof. The regenerated K_S amplitudes from two targets of the same material are made to interfere. The resulting $\pi^+\pi^-$ rate is made sensitive to Δm by varying the gap between targets (and hence the relative phase between K_S amplitudes). At high energies rather long targets are required to develop regeneration amplitudes with $|\rho| \gg |\eta_{+-}|$, which ensures minimal coupling of the Δm determination to uncertainties in $\eta_{+-}|$. For example, one meter of carbon gives $|\rho|/|\eta_{+-}| \sim 10$ at 100 GeV. The gap would have to be varied continuously (up to ~ 100 m) to obtain good systematics-free sampling of the interference.

(2) τ_S and η_{+-}. These parameters can be measured without employing regenerated K_S's by studying a neutral-K beam short enough to contain a mixture of K_S and K_L. In this case the proper-time distribution of $\pi^+\pi^-$ decays is given by[23]

$$dI^{+-}/dt = (N+\bar{N})\Gamma_S^{+-}[e^{-t/\tau_S} + |\eta_{+-}|^2 + 2D|\eta_{+-}|e^{-t/2\tau_S}\cos(\Delta m\, t - \phi_{+-})] , \tag{3.1}$$

where N ($\bar{N}$) is the number of K^0 ($\bar{K}^0$) produced at the target, $D \equiv (N-\bar{N})/(N+\bar{N})$, and τ_L has been ignored. Three comments should be made about Eq. (3.1).

(a) Since the interference term has opposite sign for K^0 and $\bar{K}^0$, the factor D is present, with $-1 \le D \le 1$. D near zero corresponds to a beam with roughly equal numbers of K^0 and $\bar{K}^0$ and results in diminished sensitivity to ϕ_{+-}, which appears only in the interference term. D near $+1$ is achieved in a proton-initiated neutral-K beam only when the K^0 has energy $> \frac{1}{2} \times$(proton energy). D near -1 can be achieved (albeit at a lower rate) with a K^- initiated beam where $(K^-,\bar{K}^0)$ charge exchange is important.

(b) Maximum statistical precision on ϕ_{+-} can be obtained by studying dI^{+-}/dt, where the two interfering amplitudes are about equal. Given $|\eta_{+-}| \sim 2\times 10^{-3}$, this turns out to be at $t \simeq 12\tau_S$. At 100 GeV/c, this corresponds to about 60 m from the target. To obtain good statistical precision on $|\eta_{+-}|$ and τ_S, it is necessary to look at $t \gg 12\tau_S$ and $t \ll \tau_S$, so a long decay volume with good acceptance for $K^0 \to \pi^+\pi^-$ decays is important.

(c) With a sufficient number of events one can determine the *shape* of dI^{+-}/dt, which is given by the expression in square brackets in Eq. (3.1). This in turn fixes $|\eta_{+-}|^2$ independent of any knowledge of the incident flux. The complete energy dependence of $|\eta_{+-}|^2$ can thus be determined in a manner that avoids the problems inherent in both the present method and that of Ref. 18. Intuitively this comes about because the proper-time distribution of $\pi^+\pi^-$ events from, say, a K^0 beam simulates that from a regenerator with $\rho = 1$. Thus η_{+-} is in effect being measured relative to an "amplitude" (unity) whose magnitude, phase, and energy dependence are precisely known.

(3) τ_L. In the theoretical context of the following paper,[3] the energy dependence of interest, in addition to those of Δm and η_{+-}, is not that of τ_S but of

$$\Gamma_L - \Gamma_S = \tau_L^{-1} - \tau_S^{-1} .$$

Thus τ_L is another K^0 parameter to be measured at high energy, one to which our present data are not very sensitive. At $p_K = 100$ GeV/c, the K_L mean decay length is approximately 3 km. Presumably one would try to measure this lifetime with the (copious) three-body decay modes of K_L. With a 50-m decay volume at $p_K = 100$ GeV/c, 10^5 K_L decays would yield τ_L with an rms uncertainty of $\sim 5\%$. Since the experiment suggested in item (4) below is predicated on obtaining a large sample of semileptonic K_L decays, these two measurements could be performed simultaneously.

(4) Another K^0 parameter which has been precisely measured at low energy[4] is the K_L semileptonic charge asymmetry δ defined in Eq. (1.2). A high-energy measurement[24] of δ would allow one to extract the slope parameter b_δ which, as shown in Sec. III of Ref. 3, is related to the other slope parameters according to

$$b_\delta \cong b_\eta - \tfrac{1}{2} b_\phi . \tag{3.2}$$

Knowledge of b_δ would thus constitute an important consistency check on measurements of b_η and b_ϕ. Recall that in the present analysis there is an ambiguity in determining b_η (because of the uncertainty in the low-energy measurements of $|\eta_{+-}|$), and the analysis of b_ϕ is complicated by strong-interaction effects. A measurement at 100 GeV of δ to, say, 4% (the precision of the world average at low energy[4]) would require the analysis of $\sim 10^8$ $K_L \to \pi l \nu$ events, which is a very large but feasible experiment. Given the values of b_η and b_ϕ quoted in Sec. II, δ might be expected at 100 GeV to increase by ~ 10—30% compared to the low-energy value.

(5) As we note in Sec. III of Ref. 3, the energy dependence of η_{+-}/η_{00} is an important piece of information, because it bears strongly on the nature of the coupling to the K^0-$\bar{K}^0$ system. As it turns out, experiments are in progress at Fermilab (experiment No. 617) and Brookhaven National Laboratory (experiment No. 749) which will be able to measure this ratio very precisely.

We have identified other K^0-decay studies which may help elucidate the precise nature of the effects reported here. These, however, are best considered in light of the theoretical analysis presented in Ref. 3, and accordingly they are discussed in that paper.

ACKNOWLEDGMENTS

This work was performed under the auspices of the U. S. Department of Energy.

APPENDIX A: KINEMATICS OF K_S REGENERATION

We review in this appendix the kinematics of the regeneration process[8] $K_L(P_L) + T(P_T) \to K_S(P_S) + T(P_T')$, where

T is the target and where the corresponding four-momenta are shown in parentheses. Using conservation of four-momentum in the laboratory frame, we find,

$$E_L - E_S = \frac{c^2(\vec{p}_L - \vec{p}_S)^2}{2M_T c^2 + E_L + E_S} , \tag{A1}$$

where $P_L = (\vec{p}_L, E_L/c)$, etc., and M_T is the target mass. For coherent regeneration in the forward direction M_T is essentially infinite, since the whole target can be thought of as producing the K_S.[25] It follows that $E_L - E_S \cong 0$ and hence

$$p_L{}^2 + m_L{}^2 c^2 \cong p_S{}^2 + m_S{}^2 c^2 . \tag{A2}$$

From Eq. (A2) we find immediately that

$$\Delta p = p_L - p_S = -\Delta m\, c^2 \frac{m}{p} , \tag{A3}$$

where $m = \frac{1}{2}(m_L + m_S)$, $p = \frac{1}{2}(p_L + p_S)$, and where p_L and p_S are the magnitudes of the corresponding three-momenta in the forward direction. Using Eq. (A3), we can verify the consistency of the approximation $E_L \cong E_S$. We note that by momentum conservation the recoil kinetic energy ΔE of a target nucleus with mass M_{nuc} is

$$\Delta E \cong \frac{(\Delta p)^2}{2M_{\text{nuc}}} \cong \frac{(m\,\Delta m\, c^2)^2}{2M_{\text{nuc}} p^2} . \tag{A4}$$

For a typical beam momentum $p = p_K = 70$ GeV/c this gives

$$\Delta E \cong 3 \times 10^{-25} \text{ eV (hydrogen)} , \tag{A5a}$$

$$\Delta E \cong 3 \times 10^{-26} \text{ eV (carbon)} , \tag{A5b}$$

$$\Delta E \cong 2 \times 10^{-27} \text{ eV (lead)} , \tag{A5c}$$

and hence ΔE is completely negligible compared to $\Delta m\, c^2$. It follows that the target nuclei act as if there were no energy transfer from K_L to K_S.

Up to this point, we have been concerned with the kinematics describing regeneration in the forward direction from a single target nucleus. For the sake of completeness we collect here some familiar results for coherent scattering away from the forward direction. Following Kleinknecht[8] we consider a K_L beam incident from the left on two target nuclei located at points A and B, as shown in Fig. 8. The phase difference $\Delta\phi$ between the two emerging K_S beams after crossing the plane C is

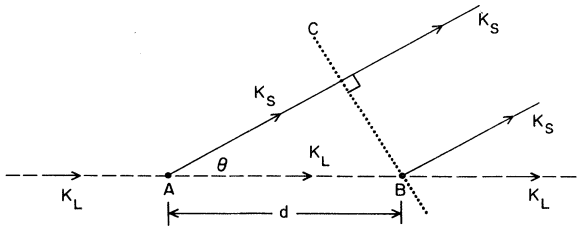

FIG. 8. K_S regeneration away from the forward direction. A K_L beam (dashed line) incident from the left scatters from either of two sites A or B located a distance d apart. The phase difference between the two emerging K_S beams after crossing the plane C is given by Eq. (A6), and the condition that these beams interfere coherently is given by Eq. (A7).

$$\Delta\phi = \frac{1}{\hbar}(p_S d \cos\theta - p_L d) , \tag{A6}$$

where d is the separation between A and B, and θ is the K_S scattering angle. Interference between the K_S beams gives rise to a factor $\cos\Delta\phi$ in the regeneration amplitude, and hence for these two contributions to be coherent we must have $\Delta\phi \lesssim 1$. Using Eq. (A3) this gives, for small θ,

$$\theta^2 \lesssim \frac{2mc^2\Delta m}{p^2} . \tag{A7}$$

From Eqs. (A6) or (2.8) we see that in the strict forward direction ($\theta = 0$), the maximum distance $d_{\max}$ over which regeneration remains coherent [$d_{\max} \mid \Delta p \mid /\hbar \lesssim 1$ or $\Delta m\, c^2 \tau_S L_{\max}/(\hbar\Lambda_S) \lesssim 1$] is

$$d_{\max} \lesssim \frac{\hbar p}{mc^2 \Delta m} . \tag{A8}$$

For a typical momentum in these experiments, $p = p_K = 70$ GeV/c, we have

$$\theta \lesssim 8 \times 10^{-10} \text{ rad} , \tag{A9}$$

and

$$d_{\max} \simeq 788 \text{ cm} . \tag{A10}$$

APPENDIX B: REGGE-POLE MODELS FOR THE PHASE OF THE REGENERATION AMPLITUDE

We discuss in this appendix several representative models of $\phi_{21}(\text{H})$ and $\phi_{21}(\text{C})$, the phases of the strong regeneration amplitudes in hydrogen and carbon, respectively. For $\phi_{21}(\text{H})$ we will consider in particular four versions of the simple Regge-pole (SRP) model and two absorption models. The models we examine have been selected because they have been extensively studied and compared to a large body of existing data. As we discuss below, $\phi_{21}(\text{H})$ is strongly constrained in such models, in part because the data of Ref. 6 for $\mid f(0) - \bar{f}(0) \mid /k$ are used in some of the fits to adjust the Regge parameters. The resulting Regge amplitudes are then used to *predict* $\phi_{21}(\text{H})$. It will be shown that all of these models predict a similar variation of $\phi_{21}(\text{H})$ in the range $35 \lesssim p_K \lesssim 105$ GeV/c, corresponding to an increase in $\phi_{21}(\text{H})$ of $\lesssim 2^0$. By way of a comparison, a linear fit to the data of Ref. 6, shown in Fig. 7, gives (p_K in GeV/c)

$$\phi_{21}^{\text{exp}}(\text{H}) = [-(139.5 \pm 6.6) + (0.28 \pm 0.09) p_K] \text{ deg} , \tag{B1}$$

corresponding to an increase in $\phi_{21}^{\text{exp}}(\text{H})$ of $(19.3 \pm 6.4)^\circ$ over the same interval.

We begin with the SRP model of Hendrick *et al.*,[26] in which the forward regeneration amplitude for $K_L p \to K_S p$, $R(K_L p \to K_S p)$, is given by

$$R(K_L p\to K_S p)=\tfrac{1}{2}[R(K^0 p\to K^0 p)-R(\bar{K}^0 p\to \bar{K}^0 p)]$$
$$=\beta^{\rho}_{Kp}\left[\tan\left[\frac{\pi\alpha_\rho}{2}\right]+i\right]p_K{}^{\alpha_\rho}-\beta^{\omega}_{Kp}\left[\tan\left[\frac{\pi\alpha_\omega}{2}\right]+i\right]p_K{}^{\alpha_\omega}. \tag{B2}$$

Here $\beta^{\rho}_{Kp}=\beta^{\rho}_{Kp}(t=0)$, $\alpha_\rho=\alpha_\rho(t=0)$, etc., $-t$ is the square of the momentum transfer, and p_K is the laboratory momentum in GeV/c. $[f(0)-\bar{f}(0)]/k$ of Ref. 6 is then related to $R(K_L p\to K_S p)$ by

$$\frac{[f(0)-\bar{f}(0)]}{k}=\frac{1}{2\pi}\frac{R(K_L p\to K_S p)}{p_K}, \tag{B3}$$

where $p_K=\hbar k$. $[f(0)-\bar{f}(0)]/k$ thus has the same units as β^{ρ}_{Kp} and β^{ω}_{Kp} which are expressed in mb. Hendrick *et al.* have fitted the nondiffractive components of various total cross sections and cross-section differences to a Regge-pole formula such as Eq. (B2), and their results are given in the first line of Table VIII. Subsequently, Bock *et al.*[6] fitted Eq. (B3) to a collection of kaon regeneration data for $|f(0)-\bar{f}(0)|/k$ in hydrogen in the range $30\le p_K\le 130$ GeV/c. Since the results of Hendrick *et al.* indicate that the ω contribution dominates over that from ρ, a fit [denoted by (A)] was performed for α_ω and β^{ω}_{Kp} with α_ρ and β^{ρ}_{Kp} fixed near the previously determined values. The results of this fit, which are given in the second line of Table VIII, are in good agreement with those of Hendrick *et al.* Bock *et al.* also performed a second fit to the same data [denoted by (B)] in which the input ρ parameters were determined from an analysis of $\pi^- p\to\pi^0 n$. The Regge parameters that emerge from this fit are given in the third line of Table VIII. More recently, Diu and Ferraz de Camargo[27] (DF) determined the ρ and ω parameters in Eq. (B2) by combining the available high-energy data for $[f(0)-\bar{f}(0)]/k$ with the experimental data for the total cross-section difference $\sigma_T(K^- p)-\sigma_T(K^+ p)$. Their results are shown in the fourth line of Table VIII. In Table VIII, we also present the results for $\Delta\phi_{21}\equiv\phi_{21}$ (105 GeV/c) $-\phi_{21}$(35 GeV/c) for the amplitudes of Hendrick *et al.*,[26] Bock *et al.*,[6] and DF,[27] along with the results of a separate fit using only the high-energy data of Ref. 6. In the latter case we have also varied the fitting procedure by fixing $\alpha_\rho=0.46$ and then determining β^{ρ}_{Kp} and α_ω for a set of values of $\beta^{\omega}_{Kp}/\beta^{\rho}_{Kp}$ from 2 to 10. All of the fits give the same value of χ^2, ~ 5.4 for 8 degrees of freedom, and hence indicate that there is a range of values for the Regge parameters which reproduce the data on $|f(0)-\bar{f}(0)|/k$. Nonetheless, we see from the corresponding predictions for $\Delta\phi_{21}$(H) that all of the models considered agree that $\Delta\phi_{21}$(H) is *small* ($\le 1.8°$) compared to the experimental value $\Delta\phi_{21}^{\rm exp}(\mathrm{H})=(19.3\pm 6.4)°$.

We turn next to the absorption model. The motivation for introducing absorption corrections into the SRP model has been reviewed at some length by Kane and Seidl[28] (KS) and more recently by Irving and Worden[29] (IW). We will thus confine the present discussion to a brief description of the absorption model so that the interested reader can follow the details of our calculation.

The absorption correction can be viewed as arising from the rescattering of the incident (final) hadrons before (after) the Reggeon exchange described by the pole contribution of Eq. (B2). The rescattering process may be either elastic or inelastic, as shown in Fig. 4 of KS, and hence various models differ on whether or how inelastic contributions are included. Since we are not concerned with those features of the data (such as polarizations and dips in $d\sigma/dt$) which are particularly sensitive to the details of various models, it is sufficient for our purposes to use a simple analytic model discussed by KS and IW. It will be shown that the parameters of this model can be adjusted to give an excellent fit to the high-energy data for $|f(0)-\bar{f}(0)|/k$. The resulting amplitude can then be used to calculate $\Delta\phi_{21}$ as we did for the SRP model. We will show that the predicted value of $\Delta\phi_{21}$ agrees not only with that obtained from the full KS absorption model, but also with the results previously obtained from the SRP model.

The amplitude $M(s,t)$ in the absorption model is given by the Hankel transform of the amplitude $M(s,b)$, where b is the impact parameter and s is the square of the c.m. energy:

$$M(s,t)=2\hat{p}_K{}^2\int_0^\infty b\,db\,J_0(b\sqrt{-t})M(s,b),$$
$$M(s,b)=R(s,b)-\frac{i}{8\pi}R(s,b)M^{\rm el}(s,b). \tag{B4}$$

Here $\hat{p}_K$ is the kaon momentum in the c.m. and J_0 is a Bessel function. $R(s,b)$ and $M^{\rm el}(s,b)$ are the (inverse) Hankel transforms of the pole term $R(s,t)$ and the elastic-scattering amplitude $M^{\rm el}(s,t)$, respectively:

$$R(s,b)=\frac{1}{2\hat{p}_K{}^2}\int_0^\infty\sqrt{-t}\,d\sqrt{-t}J_0(b\sqrt{-t})R(s,t), \tag{B5}$$

and similarly for $M^{\rm el}(s,b)$. Thus, to calculate the full amplitude $M(s,t)$ one begins by specifying $R(s,t)$ and $M^{\rm el}(s,t)$, and then transforming to find $R(s,b)$ and $M^{\rm el}(s,b)$. Since this step involves knowing $R(s,t)$ and $M^{\rm el}(s,t)$ for *all* values of t, it follows that in the absorption model (unlike the SRP model) the final expression for $M(s,t=0)$ will depend on the slope α' of the Regge trajectory $\alpha(t)$. Following KS, we take for $M^{\rm el}(s,t)$,

$$M^{\rm el}(s,t)=-is\sigma_T e^{Bt}, \tag{B6}$$

where σ_T is the total Kp cross section and $2B$ is the slope of the diffraction peak for $d\sigma(Kp)/dt$. For the pole term we use the expression for $R=R(s,t)$ given in Eq. (B2) which we rewrite using

$$\tan\left[\frac{\pi\alpha}{2}\right]+i=i\sec\left[\frac{\pi\alpha}{2}\right]e^{-i\pi\alpha/2}, \tag{B7a}$$

and

$$\left[\frac{p_K}{1\ \mathrm{GeV}/c}\right]^\alpha\approx\left[\frac{s}{2s_0}\right]^\alpha, \tag{B7b}$$

where $s_0=1$ GeV^2. Hence

$$R(s,t)=\beta(t)\left[\tan\left[\frac{\pi\alpha(t)}{2}\right]+i\right]p_K^{\alpha(t)}$$

$$\rightarrow i\tilde{\beta}(t)a(s)e^{A(s)t}\,, \tag{B8a}$$

$$\tilde{\beta}(t)=\beta(t)\sec\left[\frac{\pi\alpha(t)}{2}\right];\quad \alpha(t)=\alpha(0)+\alpha' t\,, \tag{B8b}$$

$$a(s)=[(s/s_0)e^{-i\pi/2}]^{\alpha(0)}\,,$$

$$A(s)=\alpha'[\ln(s/s_0)-i\pi/2]\,. \tag{B8c}$$

In the scattering region, $t<0$, $\sec[(1/2)\pi\alpha(t)]$ is a smooth function which can be absorbed into a redefined residue function $\tilde{\beta}(t)$. If we assume that $\tilde{\beta}(t)$ has some simple dependence such as

$$\tilde{\beta}(t)=\tilde{\beta}e^{\lambda t}\,, \tag{B9}$$

where $\tilde{\beta}$ is a constant, then Eqs. (B6) and (B8) can be combined with Eqs. (B4) and (B5) to give

$$M(s,t)=i\tilde{\beta}a\left[e^{(\lambda+A)t}-\frac{\sigma_T}{8\pi(\lambda+A+B)}\times e^{(\lambda+A)Bt/(\lambda+A+B)}\right], \tag{B10}$$

which is the final result. We observe that the absorption correction proportional to σ_T interferes *destructively* with the pole term, as it should on physical grounds. For present purposes we need $M(s,0)$ which is given by

$$M(s,0)=i\tilde{\beta}a\left[1-\frac{\sigma_T}{8\pi(\lambda+A+B)}\right], \tag{B11}$$

which depends on α' through A, as anticipated earlier. Since A is a complex function of s, it follows that the phase ϕ_{21} of $M(s,0)$ is energy-dependent, even for a single Reggeon exchange. This contrasts with the SRP model of Eq. (B2) in which the phase of each Regge pole is a constant as a function of energy, but where a variation of ϕ_{21} with energy can nonetheless arise from the combination of two or more Regge poles with different values of $\alpha(0)$. Hence for regeneration off an isoscalar target such as carbon, where only ω exchange can contribute, the SRP model predicts that ϕ_{21} is a constant as a function of energy (neglecting possible many-body effects), whereas the absorption model would lead to a small energy variation. We will return to discuss carbon in more detail below.

Table IX gives the predictions of our absorption model for $\Delta\phi_{21}$(H) for a range of values of the Regge parameters. We have set $\lambda\approx 0$ and fixed $\alpha_\rho(0)$, α'_ρ, and α'_ω at the representative values suggested by KS in their Table II. For $\sigma_T(Kp)$ we have used

$$\sigma_T(K_{L,S}p)=\tfrac{1}{2}[\sigma_T(K^+n)+\sigma_T(K^-n)]\cong 48\ \text{GeV}^{-2}\,,$$

where the data for $\sigma_T(K^\pm n)$ have been taken from Carroll *et al.*[30] B has been inferred from the data of Ref. 31 for $d\sigma(K^\pm p)/dt$. We then determine $\tilde{\beta}^P_{Kp}$ and $\alpha_\omega(0)$ for a set of values of $\tilde{\beta}^\omega_{Kp}/\tilde{\beta}^P_{Kp}$ from 2 to 10. All of the fits give $\chi^2\cong 5.4$ for 8 degrees of freedom, which is the same value found previously for the SRP model. We see from Table IX that all of the fits give similar predictions for $\Delta\phi_{21}$(H), $1.4^\circ\lesssim\Delta\phi_{21}(\text{H})\lesssim 1.6^\circ$. Moreover, these results are in good agreement with the value $\Delta\phi_{21}(\text{H})\approx 2^\circ$ obtained by KS from their full absorption model (see Fig. 9 of Ref. 28), and also with those previously obtained from the SRP model. Hence the additional energy variation of ϕ_{21}(H) introduced by absorption is far too small to account for the observed rise of ϕ_{21} in hydrogen. In summary, for the range of parameters considered in both the SRP and absorption models, we find $\Delta\phi_{21}(\text{H})\lesssim 2^\circ$, whereas the linear fit to the data in Eq. (B1) gives $\Delta[\Phi(\text{H})-\phi_{\text{geo}}]=(19.3\pm 6.4)^\circ$.

For purposes of the discussion of Sec. II, it is necessary to know not only $\Delta\phi_{21}$(H), but also the actual value of ϕ_{21}(H) in each momentum bin. In Table X we tabulate ϕ_{21}(H) as a function of p_K for the DF model, and for $\tilde{\beta}^\omega_{Kp}/\tilde{\beta}^P_{Kp}=5.6$ in the analytic absorption model. The DF parameters for the SRP model have been selected because, among the models we have considered, they are derived from the largest body of experimental data, including $|f(0)-\bar{f}(0)|/k$ itself. In the absorption model we have used the results corresponding to a residue ratio of 5.6 because this value falls in between the typical values 4.2 and 6.1 favored by DF and by Hendrick *et al.*, respectively. It should be emphasized, however, that any other set of parameters from Tables VIII or IX would lead to substantially the same results.

We complete the discussion of the hydrogen data by analyzing the energy dependence of ϕ_{21} in a more general framework. A review of various general results relating to high-energy hadron scattering has been given recently by Fischer.[32] He begins by listing a set of properties that we wish a scattering amplitude $F(z)$ to possess, where the physical energy E corresponds to positive values of Rez. For $K_Lp\rightarrow K_Sp$, these properties are embodied in a simple antisymmetric (crossing-odd) amplitude $F_A^{abc}(z)$ of the form

$$F_A^{abc}(z)=ic(-iz)^a[\ln(-iz)]^b\,, \tag{B12}$$

where a, b, and c are constants. Using (B12) one can derive various relations between the magnitude and phase of the regeneration amplitude, such as that given in Ref. 14. Fischer notes, however, that one cannot fit the combined data of Birulev *et al.*[16] and Bock *et al.*[6] with a single term of the form (B12), unless the exponent a is itself energy-dependent. This is another reflection of the rapid energy-variation of ϕ_{21}, and suggests that even if such a variation is not inconsistent with any fundamental principles, it is at the very least somewhat awkward.

Given the intimate connection between the energy-dependence of ϕ_{+-} and that of ϕ_{21} in the regeneration experiments, one can hope to extract the dependence of ϕ_{21} on energy in either of two ways. One is to measure ϕ_{+-} directly without using regeneration, as we discussed in Sec. III. The other way is to measure the energy dependence of ϕ_{21} by purely strong-interaction methods which do not depend on ϕ_{+-}. This can be accomplished by using the optical theorem to write[27]

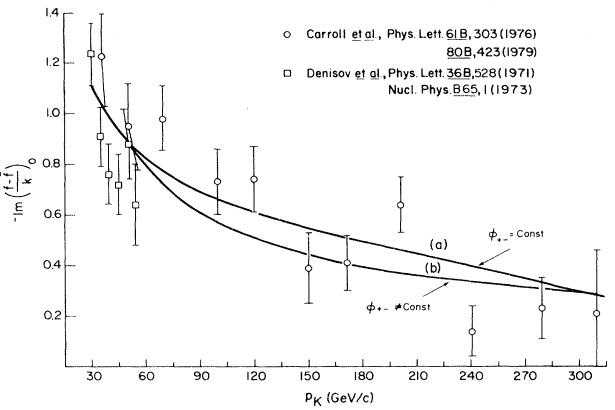

FIG. 9. $\mathrm{Im}(f-\bar{f})/k$ derived from Kn total-cross-section data. The curves are explained in the text.

$$\sigma_T(K^+n)-\sigma_T(K^-n)=4\pi\,\mathrm{Im}\left[\frac{f(0)-\bar{f}(0)}{k}\right]$$
$$=4\pi\left|\frac{f(0)-\bar{f}(0)}{k}\right|\sin\phi_{21}\ , \tag{B13}$$

where $\sigma_T(K^{\pm}n)$ are the total $K^{\pm}n$ cross sections, which are experimentally known[33,34] up to approximately 300 GeV. If we combine these data with those for $|f-\bar{f}|/k$ from Ref. 6, we can solve for $\phi_{21}(p_K)$ and compare the results to those obtained from regeneration, assuming either $\phi_{+-}=$constant or $\phi_{+-}\neq$constant. Figure 9 shows the results of such a comparison. The curve labeled (a) gives the right-hand side of Eq. (B13) under the usual assumption $\phi_{+-}=$constant. $\phi_{21}(p_K)$ is then taken from (B1) and combined with $|f-\bar{f}|/k$ from Ref. 6. By contrast, curve (b) corresponds to $\phi_{+-}\neq$constant with $\phi_{21}(p_K)$ having the much gentler energy dependence that emerges from the DF model. As we have discussed, if this energy dependence of ϕ_{21} is correct, it implies that ϕ_{+-} itself is energy-dependent. As can be seen from Fig. 9, the data are not as yet sufficiently good to distinguish between curves (a) and (b), but with a relatively modest improvement in the data such a discrimination will be possible.

Thus far, we have considered the energy variation of ϕ_{21} using only the hydrogen data. As discussed in Sec. II, data also exist for carbon and lead targets from which $\phi_{21}(p_K)$ can also be extracted in principle. In practice, however, complex nuclei give rise to additional problems which are probably not fully understood at the present time. These include inelastic contributions to multiple-scattering processes, and the form of the triple-Reggeon coupling, among others. For carbon, which is an isoscalar target, these problems are offset to a limited extent by the fact that only ω exchange can contribute, but for lead no such simplification arises.

An analysis of K_S regeneration in carbon and in other heavier nuclei has been given recently by Diu and Ferraz de Camargo.[35,36] The model developed by these authors not only includes inelastic contributions, but also allows these to proceed by the exchange of both odd and even charge-conjugation states. In Fig. 5 of Ref. 36, DF compare the predictions of their model for the momentum dependence of $\phi_{21}(\mathrm{C})$ against the experimental data of Ref. 5. Over the momentum interval, $35\leq p_K\leq 125$ GeV/c, DF predict an increase in $\phi_{21}(\mathrm{C})$ of 3°, whereas a fit to the data gives (p_K in GeV/c)

$$\phi_{21}^{\mathrm{exp}}(\mathrm{C})=[-(133.0\pm6.2)+(0.12\pm0.09)p_K]\ \mathrm{deg}\ . \tag{B14}$$

This corresponds to an increase of (11.2 ± 9.1) degrees over the same interval, and indicates that the carbon data are consistent with those from hydrogen.

We can conclude the preceding discussion with several remarks concerning the calculability of $\phi_{21}(\mathrm{H})$ and $\phi_{21}(\mathrm{C})$. From the point of view of the SRP model, the amplitude $R(K_Lp\rightarrow K_Sp)$ in Eq. (B2) is one for which Regge theory should provide a good description: To start with, the troublesome Pomeron and f do not enter while the parameters of the ρ and ω, which give the dominant contributions, can be fixed using a number of independent pieces of data on high-energy cross sections. Additionally, for coherent regeneration the residue functions β^{ρ}_{Kp} and β^{ω}_{Kp} are *constants* which can be fitted for, thus obviating the need for modeling their t dependence. Finally, the parameters of the SRP model can be fitted to the high-energy data on $|f(0)-\bar{f}(0)|/k$, which then allows $\phi_{21}(\mathrm{H})$ to be predicted. We thus see that the calculation of $\phi_{21}(\mathrm{H})$ in the SRP model is actually highly constrained, as is further evidenced by the agreement among the various results for $\Delta\phi_{21}(\mathrm{H})$ in Table VIII. By contrast the calculation of $\phi_{21}(\mathrm{C})$ requires a model of both the Pomeron and f trajectories which contribute to the elastic multiple-scattering term. In addition, various triple-Reggeon couplings are needed (see Fig. 2 of Ref. 35), as is a model of the nuclear density function. Although models can be constructed for each of the necessary components of the calculation, the resulting amplitude is necessarily much less constrained than is the case for hydrogen, and is thus correspondingly more uncertain. It should be noted that many of the aforementioned problems arise even for the simplest nuclear target, namely, deuterium, which is considered in Refs. 26 and 37.

In view of the uncertainties surrounding the calculation of $\phi_{21}(\mathrm{C})$, we have treated the carbon phase information in two ways: (a) In method A the carbon data have been combined with those from hydrogen, and the DF models[27,36] were used for both $\phi_{21}(\mathrm{H})$ and $\phi_{21}(\mathrm{C})$. Recall that in method A all the $b_x^{(N)}$ are determined simultaneously, so if the carbon data are to be used $\phi_{21}(\mathrm{C})$ is needed before any of the $b_x^{(N)}$ can be determined. (b) In method B, where all the $b_x^{(N)}$ are determined separately, we have used the combined H and C data to determine b_{Δ}, $b_{\tau S}$, and b_{η}, but for b_{ϕ} only the H data have been used. This frees b_{ϕ} from the uncertainties in the theoretical model of $\phi_{21}(\mathrm{C})$. Since $|\rho|/|\eta_{+-}|\cong 10$ for C, it follows from Eq. (2.11) that dI^{+-}/dt is dominated by the term proportional to $|\rho|^2$ in carbon. This means that the carbon data are relatively less sensitive to Φ (and hence to ϕ_{21}) than are the hydrogen data, for which $|\rho|/|\eta_{+-}|\approx 2$. Hence our results should be qualitatively similar whether or not the carbon data are used, and this conclusion is supported by Tables IV and V.

[1]S. H. Aronson, G. J. Bock, H. Y. Cheng, and E. Fischbach, Phys. Rev. Lett. 48, 1306 (1982).

[2]E. Fischbach, H. Y. Cheng, S. H. Aronson, and G. J. Bock, Phys. Lett. 116B, 73 (1982).

[3]S. H. Aronson, G. J. Bock, H. Y. Cheng, and E. Fischbach, following paper, Phys. Rev. D 28, 495 (1983).

[4]Particle Data Group (M. Roos *et al.*), Phys. Lett. 111B, 1 (1982); Particle Data Group (R. L. Kelly *et al.*), Rev. Mod. Phys. 52, S1 (1980); Particle Data Group (C. Bricman *et al.*) Phys. Lett. 75B, 1 (1978). The latter reference contains a detailed discussion of the discrepancies among various low-energy determinations of $|\eta_{+-}|$.

[5]J. Roehrig, A. Gsponer, W. R. Molzon, E. I. Rosenberg, V. L. Telegdi, B. D. Winstein, H. G. E. Kobrak, R. E. Pitt, R. A. Swanson, S. H. Aronson, and G. J. Bock, Phys. Rev. Lett. 38, 116 (1977); 39, 674(E) (1977); J. Roehrig, Ph.D. thesis, University of Chicago, 1977 (unpublished).

[6]G. J. Bock, S. H. Aronson, K. Freudenreich, A. Gsponer, W. R. Molzon, J. Roehrig, V. L. Telegdi, B. Winstein, H. G. Kobrak, R. E. Pitt, and R. A. Swanson, Phys. Rev. Lett. 42, 350 (1979).

[7]W. R. Molzon, J. Hoffnagle, J. Roehrig, V. L. Telegdi, B. Winstein, S. H. Aronson, G. J. Bock, D. Hedin, G. B. Thompson, and A. Gsponer, Phys. Rev. Lett. 41, 1213 (1978); W. R. Molzon, Ph.D. thesis, University of Chicago, 1979 (unpublished).

[8]For reviews of K^0 regeneration and K^0 phenomenology, see K. Kleinknecht, in *K-Decay: Proceedings of the Daresbury Study Weekend, 1971,* edited by A. Donnachie and D. G. Sutherland (Science Research Council, Daresbury, England, 1971), p. 75; 26, 1 (1976); Fortschr. Phys. 21, 57 (1973); J. W. Cronin, Rev. Mod. Phys. 53, 323 (1981); R. G. Sachs, Ann. Phys. (N.Y.), 22, 239 (1963).

[9]Since the PDG value of m_S is used to calibrate the magnetic field which determines the momenta of the outgoing π^+ and π^-, the low-energy value of m_S is not an independent data point, in contrast to the case for the other kaon parameters. Hence, only the energy variation of m_S is meaningful, not the low-energy intercept. For similar reasons it is possible for m_S to be energy dependent and yet appear to be constant when determined in this way. Models in which this happens will be discussed elsewhere.

[10]See Bricman *et al.* (Ref. 4) for a recent summary of the status of $|\eta_{+-}|$.

[11]M. N. Kreisler, A. M. Lopez, Y. Fukushima, D. A. Jensen, P. Surko, and J. J. Thaler, in *Proceedings of the XVIII International Conference on High Energy Physics, Tbilisi, 1976,* edited by N. N. Bogoliubov *et al.* (JINR, Dubna, U.S.S.R., 1977), p. B168.

[12]R. Devoe, J. W. Cronin, H. J. Frisch, C. Grosso-Pilcher, P. Linsay, M. J. Schochet, and D. R. Moffett, Phys. Rev. D 16, 565 (1977).

[13]One might turn the correlation evident in Table VII to advantage by asking which forms of Δm and $|\eta_{+-}|$ induce a phase variation most closely in agreement with $\Delta\Phi(\mathrm{H})$ and $\Delta\Phi(\mathrm{C})$ given in Appendix B. In fact, the second entry of Table VII, with γ^2-dependent values of Δm and $|\eta_{+-}|$ $(b_\Delta^{(2)}, b_\eta^{(2)}$ both negative) produces such a qualitative agreement. However, in making this argument we have ignored the nuclear effects in lead, taking the fitted Φ's at their face value. This is, in principle, a way of breaking the twofold ambiguity in the fits of $|\eta_{+-}|$ versus γ, γ^2 (and hence of selecting the current world average of $|\eta_{+-}|$ over the older one), but is compromised in practice by the nuclear effects.

[14]A nominal error of $\pm 4°$ has been assigned to each theoretical value of ϕ_{21}. This estimate is arrived at by fitting the hydrogen regeneration data to an effective Regge-pole formula

$$|f(0)-\bar{f}(0)|/k = A p_K^{-n},$$

where A and n are constants. $\phi_{21}=\phi_{21}(n)$ is then given by

$$\phi_{21} = -(\pi/2)(2-n),$$

from which the error on ϕ_{21} can be inferred from the error on n.

[15]M. G. Kendall and A. Stuart, *The Advanced Theory of Statistics* (Griffin, London, 1963), Vol. 2, p. 230.

[16]V. K. Birulev *et al.*, Nucl. Phys. B115, 249 (1976).

[17]The determination of $|\eta_{+-}|$ from the carbon data, quoted in the thesis cited in Ref. 5, is $|\eta_{+-}| = (2.172 \pm 0.035) \times 10^{-3}$. It should be stressed that this result, in excellent agreement with the carbon results presented here, was obtained while keeping all other K^0 parameters fixed at their accepted values.

[18]J. Roehrig, Ref. 5, p. 96.

[19]Figure 7 is reproduced from PDG (Kelly *et al.*), Ref. 4.

[20]Brandenberg *et al.* and Mugge *et al.* derive the phase from an analysis of the differential cross section for $K_L p \to K_S p$ extrapolated to $t=0$.

[21]J. H. Christenson *et al.*, Phys. Rev. 140, B74 (1965); S. H. Aronson, *et al.*, Phys. Rev. Lett. 25, 1057 (1970).

[22]M. Cullen *et al.*, Phys. Lett. 32B, 523 (1970).

[23]D. A. Jensen *et al.*, Phys. Rev. Lett. 23, 615 (1969).

[24]We thank Bruce Winstein for helpful discussions on this point.

[25]The interatomic and intermolecular forces in any target are large compared to the energy $\Delta m\, c^2 = 3.56 \times 10^{-6}$ eV required to convert K_L to K_S. Hence a macroscopic target can be thought of as a rigid object in K_S regeneration. This is even true for the liquid hydrogen target used in Ref. 6, in which the intermolecular binding energy is $\approx 10^{-2}$ eV, which is again much larger than $\Delta m\, c^2$.

[26]R. E. Hendrick, P. Langacker, B. E. Lautrup, S. J. Orfanidis, and V. Rittenberg, Phys. Rev. D 11, 536 (1975).

[27]B. Diu and A. Ferraz de Camargo F., Z. Phys. C 4, 223 (1980).

[28]G. L. Kane and A. Seidl, Rev. Mod. Phys. 48, 309 (1976).

[29]A. C. Irving and R. P. Worden, Phys. Rep. 34, 117 (1977).

[30]A. S. Carroll *et al.*, Phys. Rev. Lett. 33, 932 (1974).

[31]Fermilab Single Arm Spectrometer Group, Phys. Rev. Lett. 35, 1195 (1975).

[32]J. Fischer, Phys. Rep. 76, 157 (1981).

[33]A. S. Carroll *et al.*, Phys. Lett. 61B, 303 (1976); 80B, 423 (1979).

[34]S. P. Denisov *et al.*, Phys. Lett. 36B, 528 (1971); Nucl. Phys. B65, 1 (1973).

[35]B. Diu and A. Ferraz de Camargo F., Nuovo Cimento 47A, 495 (1978); contribution to the XX International Conference on High-Energy Physics, Madison, Wisconsin, 1980, Paper No. 0147 (unpublished).

[36]B. Diu and A. Ferraz de Camargo F., Z. Phys. C 3, 345 (1980).

[37]C. Quigg and L. L. Wang, Phys. Lett. 43B, 314 (1973).